UiT
THE ARCTIC UNIVERSITY OF NORWAY

Faculty of Science and Technology
Department of Engineering and Safety

Monitoring of Marine Ice and its Thickness for Ship Anti-/De-icing

Experimental and Analytical Study using Infrared Thermography

—

Taimur Rashid

A dissertation for the degree of Philosophiae Doctor – December 2018

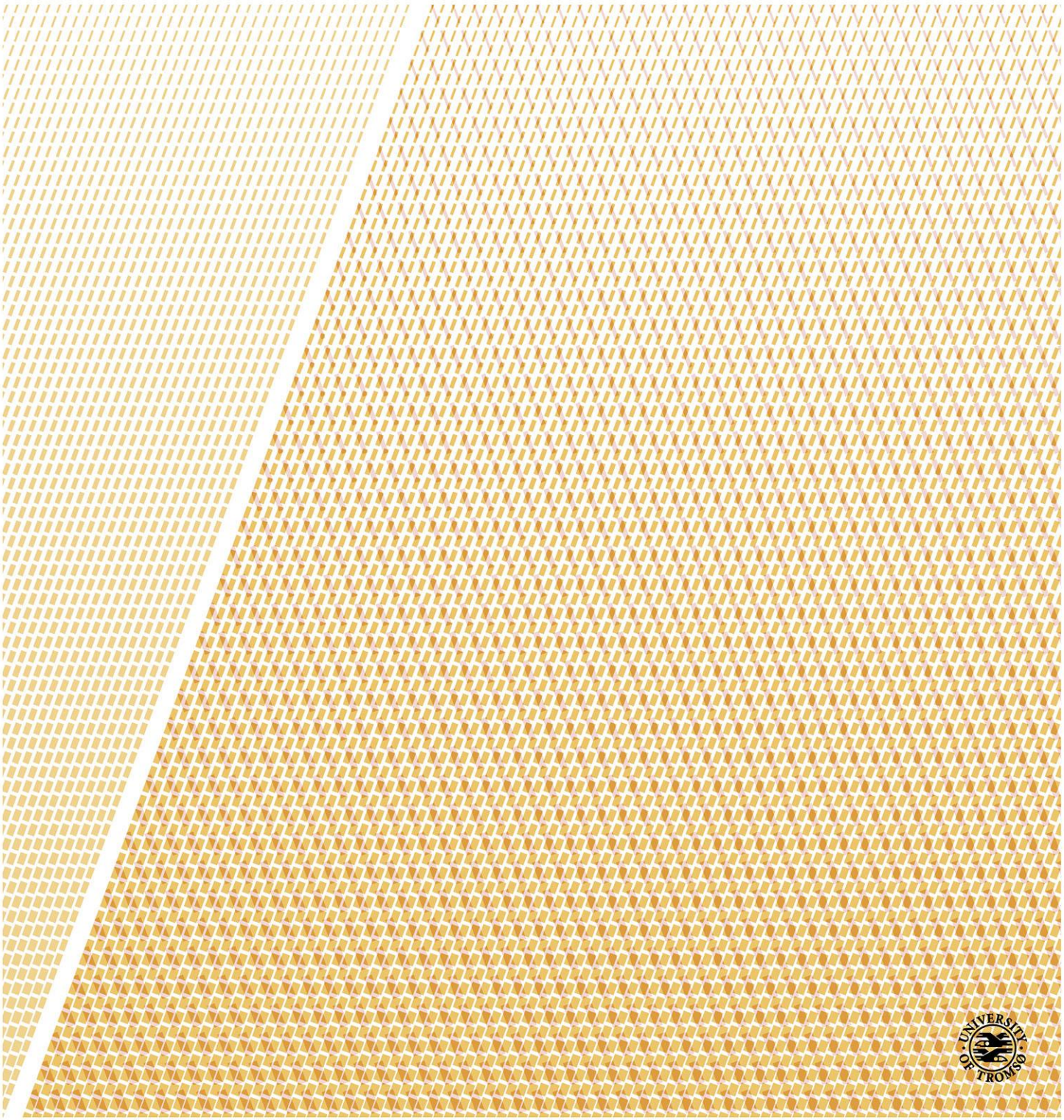

Monitoring of Marine Ice and its Thickness for Ship Anti-/De-icing

Experimental and Analytical Study using Infrared Thermography

By
Taimur Rashid

Thesis submitted in fulfilment of
the requirements for the degree of
PHILOSOPHIAE DOCTOR
(PhD)

Faculty of Science and Technology
Department of Engineering and Safety (IIS-IVT)

UiT The Arctic University of
N-9037 Tromsø
Norway
www.uit.no

ISBN: 978-82-8236-336-5
.

*To my wife, **Madiha**, my children, **Ayesha** and **Mariam**, and my parents, **Rashid** and **Fakhra**.*

"A ship in port is safe;
But that is not
what ships are built for.
Sail out to sea
and do new things."
Grace Hopper

Abstract

Ships operating in a cold climate face many challenges. There are several associated risks such as safety concerns, down time, energy consumption and limited resources. Amongst the key challenges, ship ice accretion is significant for cold climate operations. Exposing superstructures to the marine icing phenomenon can affect the ship's operations, risking the safety of humans and machines. In this regard, a set of mandatory guidelines, the International Code for Ships Operating in Polar Waters (Polar Code), was released in 2015 by the International Maritime Organization (IMO) and came into effect from 2017. Therefore, modern ships require a support system that can provide real-time information about the marine icing on different parts of the ship.

This study focuses on identifying, assessing and implementing a technique that could provide real-time information about marine ice accretion and its thickness on a surface in cold environmental conditions. In this regard, due to its particular advantages, such as non-contact measurement, area detection and the need for less observation time, infrared thermography (IRT) is used to remotely monitor the marine ice samples. Initially, the characterization of marine ice samples is performed using IRT, and experimental results are verified through numerical simulations, using a finite difference method (FDM). Thereafter, IRT is used to measure the thickness of marine ice samples when subjected to heating from underneath. The laboratory experiments are performed at controlled atmospheric conditions, and marine ice thickness up to 15mm is tested. Furthermore, an electrothermal coating material is manufactured for implementing large-scale anti-/de-icing. This is achieved by using a roll to roll (R2R) coating process of carbon nanotubes (CNTs). The coating is manufactured on a meter-scale poly(ethylene terephthalate) (PET) sheet. This R2R CNT coating is characterized and demonstrated for anti-/de-icing purposes.

The results of this study show that IRT can be used to measure the thermal properties of marine and pure ice. The effective values of thermal conductivity and overall heat transfer coefficient calculated using IRT for saline and pure ice samples agree with findings in the literature. A major finding of this study is that marine ice thickness has a strong correlation with the time taken to respond to the change in temperature, subject to heating being provided from underneath. It is also shown that marine ice thickness is empirically correlated with the rate of change of temperature and time to reach a certain temperature difference. Furthermore, a R2R CNT coating is successfully implemented on a meter-scale PET sheet, which shows linear current to voltage response. This electrothermal coating material can be used for anti-/de-icing of large surfaces.

Keywords: Anti-icing, de-icing, marine ice, infrared thermography (IRT), conductive heat transfer, marine ice thickness, cold climate, ice detection, carbon nanotubes (CNTs), electrothermal heating, roll to roll (R2R) coating

Acknowledgments

First of all, I am grateful to the Almighty ALLAH for the good health and well-being that were necessary to complete this work.

I am grateful to my wife, Madiha, for providing me with moral and emotional support in my life. She has always been keen to know what I was doing and how I was progressing throughout this research journey. I am really amazed and thankful for how she managed the additional responsibilities of the household whenever it was required.

I am grateful to my supervisor, Associate Professor Hassan Abbas Khawaja, who has provided me with tremendous support throughout this period. I really admire the way he has guided me all the way. He was always available and ready to contribute every single time I approached him.

My co-supervisor, Associate Professor Kåre Edvardsen, has always been helpful and considerate. I appreciate his valuable advice at critical moments and I am grateful for his support. I am thankful to Associate Professor Jarle A. Johansen, for his assistance and support. Also, I would like to thank my Head of Department, Tor Schive, for his administrative support, especially approving my six-month research visit to the University of Cambridge, UK, and ISO-certified training at the Infrared Training Center (ITC).

I would like to thank Dr Michael de Volder (Reader, University of Cambridge) for giving me the opportunity to work with the nano-manufacturing research group at the Institute of Manufacturing (IFM). Michael has been overwhelmingly supportive and friendly, and I felt at home during my research visit to Cambridge, UK. Very special gratitude goes to all those members of the nano-manufacturing research group at IFM. Thank you, guys! You all are amazing!

I am also grateful to the university staff, Jim Olsen, Ståle Antonsen, Karl Magnus, Arne Ketil and Gunn-Helene Turi, for their unfailing support and assistance.

Very special gratitude goes out to all of my friends, who have always listened to me carefully and encouraged me in difficult times. A very special thanks to Eirik Samuelsen, Masoud Naseri, Rezgar Zaki, Alena Dekhtyareva, Per R. Leikanger, Tanveer Ahmed and Azeem Hussain.

Taimur Rashid
Tromsø, Norway
December, 2018.

Table of Contents

Nomenclature

Symbols

c	$J/kg.K$	Heat capacity
I	A	Current
A	m^2	Area
T	K	Temperature
T_s	℃	Surface temperature
T_∞	K	Surrounding temperature
h	$W/m^2.K$	Overall heat transfer coefficient
$\dot{q}$	W/m^3	Volumetric energy generation
$q_x^{"}$	W/m^2	Heat flux
x	m	Spatial position
t	sec	Second
t_h	mm	Ice thickness
t_f	sec	Time to reach ΔT of 5ºC
t_0	sec	Time to respond
ΔT	℃	Temperature gradient
T_0	℃	Initial temperature
k	$W/(m.k)$	Thermal conductivity
$\frac{\partial T}{\partial t}$	℃$/sec$	Rate of change of temperature

Greek symbols

α	m^2/s	Thermal diffusivity
σ	$W/(m^2.K^4)$	Stefan–Boltzmann constant
ε	$dimensionless$	Thermal emissivity
λ	$W/m.K$	Coefficient of thermal conductivity
ρ	kg/m^3	Density

Abbreviations

1D	One dimensional
Ag	Silver
CFL	Courant-Fredrick's-Lewis
CNT	Carbon nanotube
CVD	Chemical vapour deposition
dc	Direct voltage
DNV	Det Norske Veritas
FDM	Finite difference method
FTCS	Forward time central space
GMT	Greenwich Mean Time
GPS	Global positioning system
IMO	International Maritime Organization
IR	Infrared

IRT	Infrared thermography
ITC	Infrared Training Centre
LWIR	Long wave infrared
MWCNT	Multiwall carbon nanotube
MWIR	Medium wave infrared
NSR	Northern sea route
PET	Polyethylene terephthalate
R2R	Roll to roll
RQ	Research question
RTP	Room temperature pressure
S	Sample
SWIR	Short wave infrared
wt.%	Percentage by weight

List of appended papers

Paper I **Rashid, T.**; Khawaja, H. A.; Edvardsen, K. "Review of Marine Icing and Anti-/De-icing Systems". *Journal of Marine Engineering and Technology 2016*; Vol. 15(2), pp. 79-87

Paper II **Rashid, T.**; Khawaja, H. A.; Edvardsen, K. "Determination of Thermal Properties of Fresh Water and Sea Water Ice using Multiphysics Analysis". *The International Journal of Multiphysics 2016*; Vol. 10(3), pp. 277-291

Paper III **Rashid, T.**; Khawaja, H. A.; Edvardsen, K. "Marine Thickness of Marine Ice Using IR Thermography". *Cold Regions Science and Technology 2019*; Vol. 158, pp. 221-229

Paper IV **Rashid, T.;** Liang, HL.; Chiodarelli, N.; Khawaja, H. A.; Edvardsen, K.; De Volder, M. "Roll to Roll CNT Coating for Electro Thermal Heating". Manuscript ready.

Additional papers, not included

Paper V **Rashid, T.;** Khawaja, H. A.; Edvardsen, K. “Ice Detection of Pure and Saline Ice Using Infrared Signature”. Sensors & Transducers Journal 2016; Vol. 206(11), November 2016, pp. 82-87

Paper VI **Rashid, T.;** Khawaja, H. A.; Edvardsen, K.; Mughal, U. N. “Infrared Thermal Signature Evaluation of a Pure and Saline Ice for Marine Operations in Cold Climate”.

Paper VII **Khawaja, H. A.;** Rashid, T.; Eiksund, O.; Broadal, E.; Edvardsen, K. “Multiphysics Simulation of Infrared Signature of an Ice Cube”. The International Journal of Multiphysics 2016; Vol. 10(3), pp. 291-302

Part I – Thesis Summary

1.Introduction and background

The Arctic region has become a region of interest for many stakeholders. These stakeholders involve policy makers, oil and gas enterprises, tourism, fishing merchants, the renewable energy industry, the mining sector, researchers and the indigenous population. The interest has led to commercial activity, which is continuously on the rise inside the region (Jensen, 2008). The Arctic includes Barents Sea, Alaska, northwest and east Russia, eastern Canada and the Green shelf (Figure 1). The commercial activity has stimulated the maritime and shipping operations. For instance, the statistics from Miller and Ruiz (2014) show that northern sea route (NSR) transit had increased by 20% from 2009 to 2013. However, maritime operations in cold climates are not easy, and there are various challenges, compared to the normal weather maritime operations (Marchenko, 2012). These challenges can be summarized as harsh weather conditions, machine and human safety, limited support, inadequate infrastructure and a sensitive ecosystem (Makkonen, 1984; Ryerson, 2011; Shellard, 1974; Ayele and Barabadi, 2016).

Figure 1: Arctic region

Harsh weather conditions constitute the key contributing factor affecting shipping operations in cold climate regions. In the Arctic Ocean, various accidents have been reported (Marchenko, 2012), the major cause of which has turned out to be the climate, along with human factors. Considering climatic factors, marine icing is a well-known phenomenon affect maritime operations. It is necessary for the safety of humans and ships to be ensured in such severe icing conditions (Figure 2). In this regard, the International Maritime Organization (IMO) has taken several steps to improve shipping safety standards in polar waters and a guideline was introduced in 2002 (IMO, 2002). In recognition of the need to improve the standards, provision for ship ice mitigation was introduced in the IMO's set of guidelines in the International Convention for the Safety of Life at Sea – SOLAS (IMO, 2004). The most significant development was made in 2015, in order to improve the IMO's set of guidelines. An improved version of the International Code for Ships Operating in Polar Waters (Polar Code) was released in 2015 (IMO, 2015). The aim of the Polar Code was to increase ship safety and reduce the social/environmental impact due to shipping operations in polar waters (IMO, 2015). The Polar Code addresses a wide range of issues, especially ice mitigation and removal.

Figure 2: Ice accretion on a ship (Photo credit: Norwegian Coast Guard/Håkon Kjøllmoen)

The icing on ships and offshore structures is caused by two factors: namely, atmospheric sources and sea spray. The atmospheric sources include *freezing rain*, *supercooled fog* and *snow* (Foder, 2001; Fikke et al., 2006). Sea spray is generated by wave collisions, waves breaking due to strong winds and bursting bubbles floating on waves (Lozowski E.P, 2000; C.D O'Dowd, 2008). Marine ice accretion can be a threat to a ship's safety by affecting its stability and equipment (Wiersema et al., 2014).

The mitigation of ice, particularly that generated from sea spray, becomes significant for ensuring safe operations in cold climates. Although it is difficult to predict the level of icing on marine platforms, attempts increased after the 1940s, when several ship accidents were reported (Sawada, 1968; Shellard, 1974). Samuelsen (2017) has comprehensively described the evolution of ship-icing prediction methods, starting from the 1960s, when

icing was included in the [1]SYNOP code for weather observation (WMO, 1962). Thereafter, several icing nomograms were developed (Sawada, 1962; Mertins, 1968). The nomograms by (Mertins, 1968), Wise (1980); (Comiskey et al., 1984) and Overland et al. (1986) were developed from the data collected from ships operating in the oceans of Japan and Canada, the Gulf of Alaska and northeast of the Pacific Ocean. In addition, numerical prediction models from wave-ship interactions were developed from the 1970s (Kachurin et al., 1974) and, to date, they are being continuously improved (Comiskey et al., 1984; Roebber and Mitten, 1987; Zakrzewski et al., 1988; Horjen, 2013; Dehghani et al., 2017; Fazelpour et al., 2017; Samuelsen et al., 2017). These available ice prediction models are derived from input parameters relating to atmospheric conditions such as wind speed, sea surface temperature and air temperature.

Ice prediction models are one of the means to mitigate ship icing. In addition, there are several anti-/de-icing methods to reduce ice accretion on ships. Most of these methods have evolved from procedures in the aviation, electric and transportation industries that are adaptable to the marine environment (Ryerson, 2011). Ship sections can also be prioritized in different categories and anti-/de-iced with respect to the implication of the safety standards. Det Norske Veritas (DNV) classifies ship equipment and parts into two major categories, the first of which includes navigation, propulsion, anchorage, steering and life-saving equipment. It is recommended that these items are anti-iced under all conditions during operation. The second category includes superstructure, deck, railings, helipad and cargo deck area. Equipment in this category can be de-iced within 4–6 hours after ice accretion. Almost 15 classes of de-icing and anti-icing technologies have been identified for marine platforms (Ryerson, 2009), most of which involve chemical, thermal and mechanical methods. Amongst them, some technologies are in the development phase. In addition to manual techniques, anti-/de-icing technologies can be active or passive, categorized on the basis of being with or without power requirement. For instance, heat is a traditional active source of anti-/de-icing.

Overall, there is no single technology that could satisfy the entire anti-/de-icing needs of a ship (Ryerson and Tripp, 2014). This is due to the diversity in the ship's operations, its size and shape and the type of ice formed.

1.1. Research motivation

The anti-/de-icing of ships operating in a cold climate is a key challenge for the shipping industry. There are several risks associated with the anti-/de-icing such as safety concerns, down time, energy consumption and limited resources. This thesis is a part of a [2]MAROFF programme, entitled "Optimization of Ship Operations in Arctic Waters by Application of Sensor Technologies for Ice Detection, De-icing and Weather Data". This MAROFF programme is focused on ice protection for ships and is a co-operation between the University of Tromsø and its industrial partners linked to the shipping industry. The thesis work is related to the programme's work package that deals with the development of a

[1]A numerical code used for reporting weather observations made by manned and automated weather stations.
[2] Maritime Activities and Offshore Operations – MAROFF. A programme of Norwegian research council

decision-support system, with the capability of giving an early warning about the risk of icing accretion (MAROFF, 2013). Although the decision support system of a particular ship can be supported with better forecasts of icing for days or weeks (Samuelsen, 2017), there is also a need for a support system that could give real-time information about the marine icing on different parts of the ship. This information on marine icing could assist the ship's officers to take necessary actions in the case of severe ice accretions. At present, marine icing on ships is removed through traditional manual methods and/or by applying heat to the surface in order to anti-/de-ice. Real-time monitoring of marine icing on ships can also help the forecasting methods on the ships, ultimately strengthening the decision-support system of ships operating in a cold climate.

1.2. Problem statement

Exposing ship superstructures to marine icing phenomenon can affect operations, risking human and machine safety. The response time to take appropriate measures in moderate to severe ice accretion is critical, in order to minimize the risk. The traditional anti/de-icing systems are inadequate to address this issue appropriately. Hence, an efficient support system is required for anti/de-icing mechanisms. Furthermore, traditional anti/de-icing systems consume a lot of energy in heating the superstructures, as they are powered on during the entire operation, irrespective of the presence of ice.

This requires an engineering solution that would give a realistic picture of the marine icing phenomenon occurring on a ship. The support system would improve efficiency, if this solution were to contribute to providing key information about the presence of ice. To my knowledge, no solution exists to date, to remotely monitor marine icing, including the marine ice thickness, in real time on ships. Hence, there is need for an engineering solution for the shipping industry that is efficient, energy-saving and capable of monitoring the real-time picture of the marine icing phenomenon on superstructures.

This study attempts to provide an engineering solution, as it focuses on validating and implementing a remote sensing technique infrared thermography (IRT) to monitor the marine icing conditions on the superstructures. This study provides the methodology for detecting the phenomenon of marine icing, along with the thickness of the icing. It also includes the manufacturing and testing of an electrothermal coating material from carbon nanotubes (CNTs) for anti-/de-icing purposes.

1.3. Research questions

The research problem of this study focuses on identifying, assessing and implementing a technique that could assist in providing real-time information on marine ice accretion and its thickness on a surface in cold environmental conditions. This research problem is narrowed down to produce the following research questions:

RQ1 How is ship icing generated, and what are the existing anti-/de-icing systems to mitigate the marine ice?
RQ2 Is infrared thermography (IRT) a viable technique to monitor cold objects? How is this technique (IRT) used to characterize the thermal properties of marine ice?
RQ3 How can marine ice thickness be remotely detected/measured using IRT?
RQ4 How can active heating on a large scale be implemented for anti-/de-icing?

1.4. Research objectives

The research questions from the above lead to the following research objectives of this study:

1. Understand the marine icing phenomenon and the existing tools, techniques and methods used to mitigate icing on ships.
2. Perform infrared thermography (IRT) and simulation analysis, in order to characterize the thermal properties of marine ice, in comparison with fresh water ice.
3. Perform controlled experimentation, using IRT, to measure the marine ice thickness and its correlated parameters.
4. Manufacture and test a customized electrothermal coating to demonstrate the anti-/de-icing capability.

1.5. Scope of the research

The scope of this study is to remotely monitor the marine ice thickness using IRT. The characterization of marine ice samples is experimentally tested and verified using IRT. After the characterization of marine ice, experimentation is performed in controlled climatic conditions to measure the marine icing thickness. The methodology of this study is developed and implemented, taking into consideration the assumption that marine ice starts to accrete, or it has already accreted on a surface. Area-observation of marine ice samples is performed, in comparison with point-observation measurements. The methodology is developed, keeping in view the ship's superstructure, such as decks, pathways, stairs etc., where it is not feasible to place point sensors.

1.6. Limitations

- The results of this study are only based on laboratory experiments.
- All experiments are performed using IRT with only long wave infrared (LWIR) cameras, with a spectral range of 8µm to 13µm.
- The marine ice used is prepared experimentally by freezing the sea water in a freezer.
- Ice properties were determined under natural convection at RTP. Conduction in the ice is thermal, in conjunction with convection and radiation to the surrounding

environment. Effective values of thermal conductivity and overall heat transfer coefficient are used (not the absolute values).

- This study is limited to observing the thermal properties of marine and pure ice samples, measuring marine ice thickness up to 15mm.

- The ice samples for measuring thickness are prepared and only observed on a flat surface.

- The marine icing thickness parameters are observed inside a simulated cold climate environment.

- The marine ice thickness computed from experimentation can slightly vary if the method is implemented on a real platform i.e. on a ship's structure. The calibration will then be required on a real platform. This calibration will depend upon certain factors such as the salinity of the ice, trapped air within the ice, viewing angle of the installed IR camera, and the installation/thermal specifications of the heating elements and the insulating materials placed underneath.

- A qualitative anti-/de-icing demonstration of roll to roll (R2R) CNT coating is only performed inside the cold room and in atmospheric conditions.

2. Research methodology

This study focuses on identifying, assessing and implementing a technique that could assist in providing real-time information about marine ice accretion including its thickness on a surface in cold environmental conditions. The phenomenon of severe ice accretion during marine operations is mainly caused by sea spray and atmospheric factors, with sea spray icing being a major contributor to icing on ships/offshore structures. Paper I discussed the various theoretical and experimental models for predicting the icing rate that deal with the specific set of parameters in a particular environment. In addition, various anti-/de-icing technologies have been reviewed and it has been found that no single anti-/de-icing technique can satisfy the entire ice protection requirements of a ship or an offshore platform. This is because the ice accretion phenomenon in cold regions is complex and more localized and reliable ice detection is required to support anti-/de-icing systems.

2.1. Introduction to infrared thermography (IRT)

Infrared (IR) radiation lies in the band of the electromagnetic spectrum between the wavelengths of 0.7µm to 1mm. The IR band is subdivided into short wave IR (SWIR), ranging from 0.9 µm to 1.7µm, medium wave IR (MWIR), ranging from 1µm to 5µm, and long wave IR (LWIR), ranging from 8µm to 13µm. The infrared spectrum is shown in Figure 3.

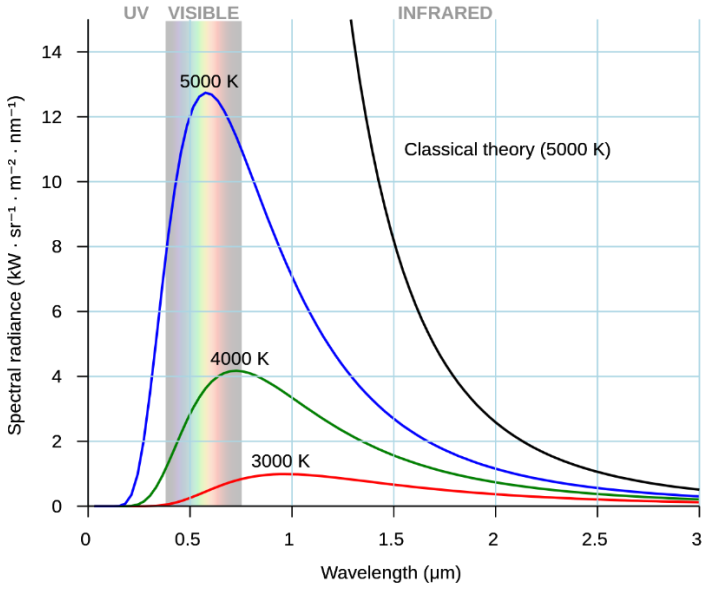

Figure 3: IR Spectrum

The thermal radiation emitted from many objects exists in the infrared region. This is due to the fact that all physical objects above absolute zero (zero kelvin) will emit some radiation, regardless of the state of matter, i.e. solids, liquids and gasses. Plank's law (Eq. (1)) gives us the spectral energy (B_λ) per steradian per square meter of area and per meter of wavelength (λ).

$$B_\lambda(Watt.sr^{-1}.m^{-3}) = \frac{2hc^2}{\lambda^5}\frac{1}{e^{\frac{hc}{\lambda k_B T}}-1} \quad (1)$$

where h is Planck's constant ($6.6x10^{-34}J/s$), k is Boltzmann's constant ($1.4x10^{-23}J/K$) and c is the velocity of light $2.99x10^{8}m/s$.

Differentiating Eq. (1) gives us the wavelength at which the spectral energy is at its maximum value (λ_{max}). This is Wien's law, as given in Eq. (2).

$$\lambda_{max}(\mu m) = \frac{2898}{T(K)} \quad (2)$$

The total amount of energy (W) radiated from the object can be obtained by integrating Eq. (2), which gives us the Stefan–Boltzmann law, as shown in Eq. (3).

$$W(Watt.m^{-2}) = \epsilon\sigma T(K)^4 \quad (3)$$

where ε is the emissivity, i.e. the ratio with respect to black body (dimensionless), σ is the Stefan–Boltzmann constant ($W/(m^2.K^4)$ and T is the surface temperature (K).

Infrared cameras are used to detect the emitted radiation from the surface of a target object and translate into a visual image. This image contains the information of the surface temperature of the target object that can be post processed for further analysis.

2.2. Feasibility of IRT for remotely monitoring marine icing

In marine operations, remote detection of icing can be effective, as it can assist in the detection of a larger surface area. In order to remotely monitor the marine icing on a surface area, infrared thermography (IRT) is a viable technique. IRT has certain advantages such as non-contact measurement, non-destructive testing, area detection and less observation time. Remote monitoring of ice upon surfaces has been tested in the aviation industry, where icing on aircraft wings was observed using infrared cameras (Gregoris et al., 2004). The effectiveness of IRT in marine ice accretion on superstructures needs to be investigated. Specific infrared cameras are currently being used in marine operations to detect icebergs floating in the sea; this indicates the possible applicability of infrared devices in the marine environment (FLIR®, 2016).

IRT has a common application in observing high-temperature objects. High-temperature objects emit more radiation, resulting in a higher photon count that collides with the surface of the infrared (IR) sensor. Therefore, it is much easier to detect high-temperature objects with IRT. On the other hand, the colder objects contribute to less infrared emissions. In this case, an object's emissivity and environmental factors become all the

more significant. However, ice is a good emitter of IR radiations, with the emissivity lying in the range of 0.8 to 0.95 (Figure 4), based on its formation and freshness, with zero being a poor emitter and 1 being highly emissive.

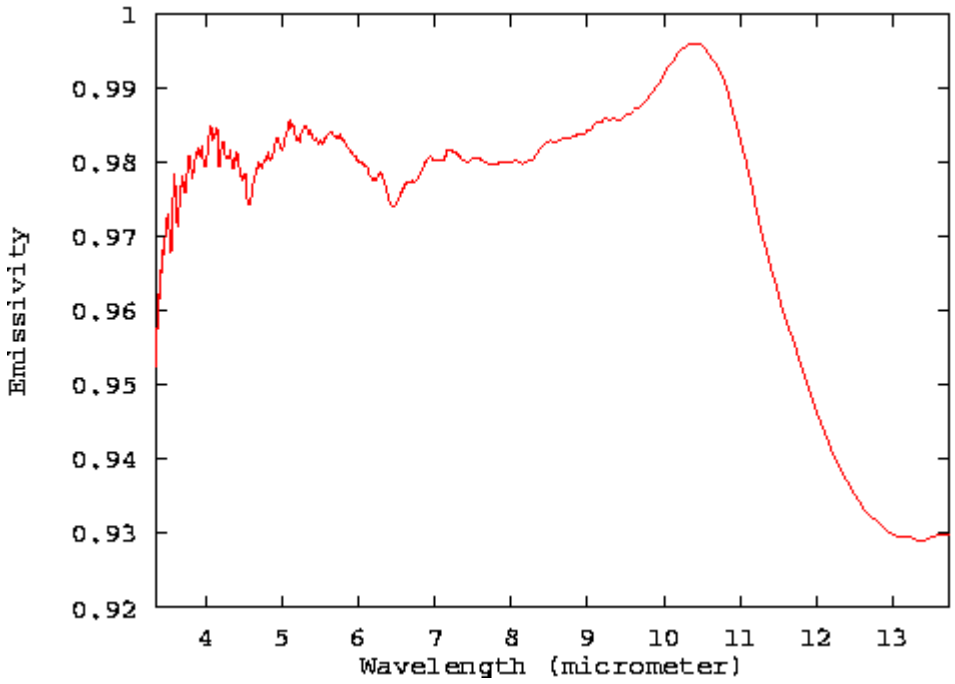

Figure 4: Emissivity of ice with wavelength (μm) (Zhang, 1999; Khawaja et al., 2016)

In contrast to measuring high-temperature objects, IRT has also been used to observe cold objects such as snow, freezing lakes and pure and saline ice (Barber et al., 2014; Rashid et al., 2015; Rashid et al., 2016; Hori et al., 2013; Shea and Jamieson, 2011; Fazelpour et al., 2016). In a controlled experimental setup, marine ice can be identified and its thermal gradients can be observed using IRT as reported in the preliminary work of this study (Rashid et al., 2015; Rashid et al., 2016). Figure 5 shows an illustration of IRT on the top surface of a random marine ice sample, in comparison with a pure ice sample when allowed to warm up naturally through natural convection. Figure 5 shows that IRT can be used to observe the surface temperature of marine ice in a controlled environmental setup. This is demonstrated in Paper II and Paper III. Moreover, the thermal conductivity of marine ice can also be computed and verified using IRT (Paper II).

2.3. Salinity of marine icing samples used in the study

Marine ice samples used in the study were prepared from seawater collected from Norskhavet (GPS 69°41'07.2"N 19°00'23.3"E). Controlled laboratory tests were performed to measure the salinity. The average salinity of five samples is shown in Table 1. The salinity of seawater sample was calculated as 46.4±0.9 g/l.

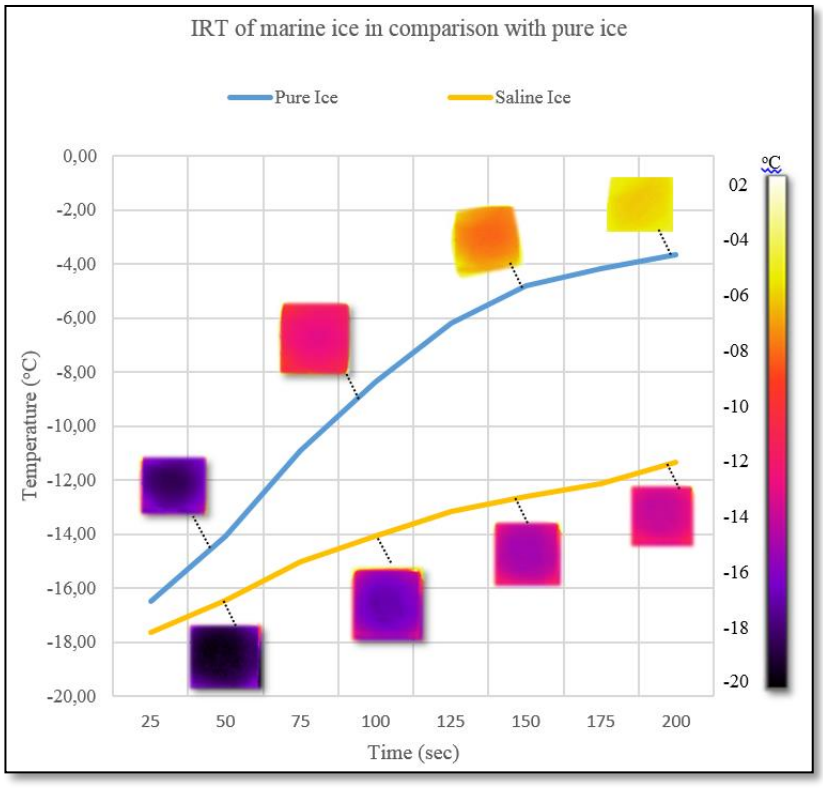

Figure 5: IRT of marine ice samples' top surface, in comparison with the pure ice sample subjected to similar conditions (adopted from (Rashid et al., 2015))

Table 1: Salinity of marine icing samples used for experiments

Salinity Calculation							
Sample	**Empty wt. container (g)**	**Seawater + container (g)**	**Dried wt (g)**	**Salt + water (ml)**	**Water only (litre)**	**Salt wt. (g)**	**Salinity (g/litre)**
1	176.8	245	179.8	68.2	0.0652	3	46.0
2	180	249	183	69	0.066	3	45.5
3	178	248	181.2	70	0.0668	3.2	47.9
4	178.8	247.3	181.8	68.5	0.0655	3	45.8
5	178.7	249.9	181.9	71.2	0.068	3.2	47.1
				Average			**46.4**
				Standard Deviation			**0.9**

IRT is the focal point of this study, and the author has professional training in thermography (Category 1 Thermography ISO18436, Category 2 Thermography ISO18436, and Category 3 Thermography ANSI/ASNT CP- 105).

3. Discussion of the results

This chapter discusses the results relevant to research questions of this study. These results include the numerical simulations and experimental findings. In addition, a qualitative demonstration of an electrothermal coating for anti-/de-icing is presented.

Section 3.1 discusses sea spray icing in marine operations and ongoing/developed methods to mitigate icing conditions (Paper I). In Section 3.2, results are discussed in relation to marine and pure ice's thermal conductivity, obtained experimentally using IRT, and its verification through numerical simulation (Paper II). In Section 3.3, the results are related to measuring the marine ice thickness from IRT, including the correlated parameters (Paper III). Section 3.4 presents the electrothermal characterization and anti-/de-icing performance of R2R CNT coating (Paper IV).

3.1. Paper I

Review of Marine Icing and Anti-/De-icing Systems
Rashid, T.; Khawaja, H. A.; Edvardsen, K. *Journal of Marine Engineering and Technology 2016*; Vol. 15(2), pp. 79-87

The number of operations in cold regions has increased, due to oil exploration and other interests. The phenomenon of severe ice accretion during marine operations is mainly caused by sea spray and atmospheric factors, with sea spray icing being a major contributor to icing on ships/offshore structures. The main source of sea spray icing is the spray generated by collisions between the structure and waves. The phenomenon of *sea spray* ice accretion begins to occur after the generation of sea spray, when the air temperature drops below the freezing point of seawater (approximately –2 °C). As shown in Figure 6, the airborne liquid water droplets carried by cold air impinge on the structure, creating ice, followed by a liquid water film. With the growth of ice thickness, sea salt precipitates, creating pure ice and brine pockets. Under gravity, the liquid water film drains as runoff water. In such cases, the majority of water upon impact is drained off from the icing surface, and only a small amount is entrapped; this process of ice growth on a structure is known as *wet growth* (Makkonen, 1987).

Theoretical and experimental models for predicting the icing rate deal with the specific set of parameters in a particular environment, and, hence, they are difficult to generalize for all sorts of shipping platforms and sea conditions.

Ice can be detected using a variety of technologies, which sense the presence of ice, based on its mass, electrical and thermal properties. These devices are specific to the operational

environment and the area of application, e.g. point detection, event occurrence, mass, rate, etc.

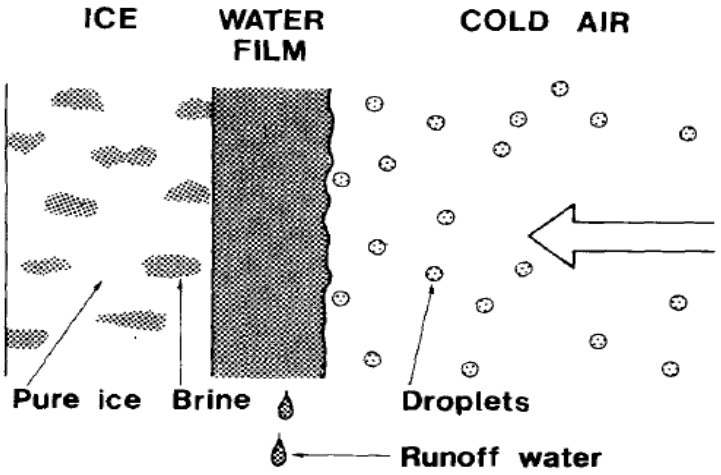

Figure 6: Sea spray icing accretion phenomenon (Makkonen, 1987) in Figure 1 of Paper I

Homola et al. (2006) categorized ice detection using direct and indirect methods and reviewed various available ice detectors. Ryerson (2011) discussed four ice detection technologies, which include imaging, remote sensing, conformal and probe detection methods, and highlighted that remote imaging ice detection could be implemented in areas of ships and offshore platforms such as decks, stairs and open working areas. Foder (2001) issued a standard for ice accretion on all kinds of structures, except for electric overhead line conductors. A comprehensive review of ice detection devices is provided by Fikke et al. (2006), as shown in Table 2. This work includes ice detection requirements from the perspective of available standards, experience from icing data collection/measurements and long-term recommendations for icing measurements.

The key finding of Paper I is that no single anti-/de-icing methodology can satisfy the entire ice protection requirements of a ship or an offshore platform (Ryerson and Tripp, 2014). The ice accretion phenomenon in cold regions is complex and more localized; it requires reliable ice monitoring to support anti-/de-icing systems. Ice detection techniques work on various physical properties such as mass, liquid water content, electrical and thermal properties, etc. Some of these properties are used in commercially available ice detectors, while work to develop more reliable ice detectors is ongoing.

Table 2: List of available ice detectors (Fikke et al., 2006) in Table 4 of Paper I

S. No.	Instrument	Manufacturer	Technique
1.	Rosemount 0872J / 0871LH1	Goodrich (USA)	Vibrating rods
2.	Rosemount 872C2 (ASOS-USA)	Goodrich (USA)	
3.	SYGIVRE (Icing Rate Meter (IRM))	Hydro Quebec – Transénergie (CA)	
4.	Vibrometer (Prototype)	Boschung (CH)	
5.	Infralytic IR detector (Prototype)	Infralytic (D), MeteoSwiss (CH)	Direct back-scattering of infrared beam
6.	T21, T23 and T26	HoloOptics (SE)	Infrared beam reflected on surface
7.	ICEmeter	IAP (CZ)	Weight measurement
8.	METEO device	EGU (CZ)	
9.	IceMonitor	Combitech (SE)	
10.	ICECylinder (Prototype)	FMI (FI)	
11.	EAG 200	No longer manufactured	
12.	Rotating Multicylinder (Prototype)	VTT (FI), STATNETT (NO)	LWC and droplet size measurement
13.	Gerber	Gerber Scientific Inc. (USA)	
14.	Labko LID-3210C	Wavin-Labko (FIN)	Active/passive microwave
15.	Instrumar IM101 V2.4	Instrumar Inc. (CA)	Electrical impedance based
16.	Jokkmokk	Segerström (SE)	Light obstruction
17.	IceMeister	www.newavionics.com	

3.2. Paper II

Determination of Thermal Properties of Fresh Water and Sea Water Ice using Multiphysics Analysis
Rashid, T.; Khawaja, H. A.; Edvardsen, K. *The International Journal of Multiphysics 2016*; Vol. 10(3), pp. 277-291

The results presented in Paper II demonstrate the characterization of marine ice samples, using IRT and numerical simulations. In this regard, successful experiments were performed to measure the variations in the surface temperatures of marine ice samples using IRT. Finite difference method (FDM) simulations were performed to compare the coefficient of thermal conduction (also known as thermal conductivity) and the overall heat transfer coefficient (the amount of heat transfer, based on the temperature difference between the two points), using Eq. (7) and Eq. (8) which are shown later. For comparison purposes, a pure ice sample was included in the experimentation and the simulation process.

Variations in the surface temperatures of marine and pure ice were observed experimentally using IRT, and the setup is shown in Figure 7. These variations depend on two primary heat transfer parameters: namely, conductivity of ice within the icing block and overall heat transfer coefficient. The heat equation is represented in Eq. (4), which can be numerically solved using the boundary and initial conditions.

$$\rho c \frac{\partial T}{\partial t} = \dot{q} + \frac{\partial}{\partial x}\left(k \frac{\partial T}{\partial x}\right) \tag{4}$$

Where ρ is density of the medium (kg/m^3), c is specific heat $(J/(kg.K))$, $\dot{q}$ is the volumetric energy generation term (W/m^3), T is the temperature (K), x refers to the spatial position (m), k is the coefficient of thermal conductivity $(W/(m.k))$ and t is the time (s).

The convective boundary conditions are applied on each external icing surface of the cubical geometry, as shown in Eq. (5).

$$-k \frac{\partial T_s}{\partial x} = h(T_\infty - T_s) \tag{5}$$

where T_s is the surface temperature (K), T_∞ is the surrounding temperature (K) and h is the convective heat transfer coefficient $(W/(m^2.K))$.

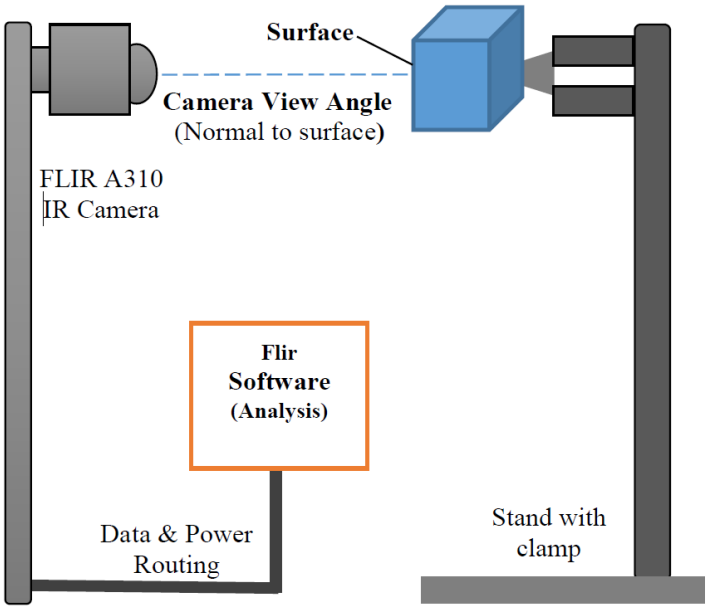

Figure 7: Testing the feasibility of IRT for observing marine ice thermal gradients, in Figure 4 of Paper II

The finite difference method (FDM) is used to numerically solve the heat equation (Eq. (4)). This method approximates the differentials with differences by discretizing the dependent variables (temperature, in this case) in the independent variable domains (space and time, in this case) (Patankar, 1980). The individual discretized value of the dependent variable is referred to as a nodal value. In the numerical simulation, the heat equation is discretized using a Forward Time Central Space (FTCS) FDM. The discretized equation is given in Eq. (6).

$$\begin{aligned} T_{i,j,k}^{t+1} = T_{i,j,k}^{t} &+ \alpha \frac{\left(T_{i+1,j,k}^{t} - 2T_{i,j,k}^{t} + T_{i-1,j,k}^{t}\right)}{(\Delta x)^2} \Delta t \\ &+ \alpha \frac{\left(T_{i,j+1,k}^{t} - 2T_{i,j,k}^{t} + T_{i,j-1,k}^{t}\right)}{(\Delta y)^2} \Delta t \\ &+ \alpha \frac{\left(T_{i,j,k+1}^{t} - 2T_{i,j,k}^{t} + T_{i,j,k-1}^{t}\right)}{(\Delta z)^2} \Delta t \end{aligned} \tag{6}$$

where α is the thermal diffusivity term (m^2/s). The superscript t and subscripts i, j, k refer to time and position for a value of nodal temperature, respectively. Δt is a time step size (s) and $\Delta x, \Delta y, \Delta z$ are the differences in the spatial positions of the temperature nodes.

The boundary condition is also discretized using the FDM, but only applied to the outer surfaces, as shown in Eq. (7).

$$-\lambda \frac{\left(T_{i+1,j,k}^{t} - T_{i,j,k}^{t}\right)}{\Delta x} = h(T_{\infty} - T_{i,j,k}^{t}) \tag{7}$$

where λ is the coefficient of thermal conductivity $(W/(m.k))$.

For the stability and accuracy of FDM, it is necessary to choose the correct time step value. The courant-Fredrick's-Lewis CFL condition (Patankar, 1980; Courant et al., 1928) is used to decide the time step size in the simulations. The CFL condition for the heat equation is given in Eq. (8).

$$2\alpha\Delta t \leq (\Delta x)^2 \tag{8}$$

The thermal properties of marine and pure ice were simulated by solving Eq. (6) and (7) and post-processing in MATLAB® (MATLAB®, 2015). The simulated values of thermal conductivities of ice and its temperature variations with time are compared with the IR images.

3.2.1. Coefficient of thermal conduction

The coefficient of thermal conduction (also known as thermal conductivity) determines the amount of heat transfer, based on the temperature difference between the two points. Figure 8 and Figure 9 show the variation in the temperature of the fresh water and saline water ice cubes, respectively. Table 3 gives the corresponding values of thermal conductivity.

Table 3: Coefficient of Thermal Conduction of Fresh Water and Saline Water Ice in Table 1 of Paper II

Coefficient of Thermal Conduction of Ice (λ)	**Value (W/(m.K))**
Fresh Water Ice	2.35
Saline Water Ice	0.8

The coefficient of thermal conductivity of fresh water ice is found to be in agreement with the literature (Petrenko and Whitworth, 2002). The coefficient of thermal conductivity of saline water ice is found to be less than the values stated in the literature. The reason for such behaviour can be explained by the fact that the saline ice started to melt far earlier in the experiments. This created a layer of water around the ice cube, hence reducing the effective thermal conductivity of the ice cube. The thermal conductivity of saline water is in the range of 0.5-0.7 (W/(m.K)) (Ramires et al., 1995). The thermal conductivity varies with temperature; however, the experimentation results show the average values over a temperature range (-30°C to 0°C). The temperature contours are not symmetric in experiments, as can be seen in Figure 8b and Figure 9b. This can be associated with the influence of buoyancy.

3.2.2. Coefficient of overall heat transfer

The coefficient of overall heat transfer (also known as the overall heat transfer coefficient) determines heat flux from one body to another. In the given case, the overall heat transfer coefficient determines the amount of heat energy being transferred from the surroundings to the ice cubes. In order to calculate the heat transfer coefficient, the variation in temperature is monitored on the ice cube surface. Figure 10 and Figure 11 show the

variation in temperature for the fresh water and saline water ice cubes in time. Table 3 gives the corresponding values of thermal conductivity.

The results indicate that the heat transfer coefficient of fresh water ice is almost twice that of saline water ice under the same room conditions. This can further be linked to the observation that saline water ice started to melt in the initial stages and, hence, built a coat of water on the ice, consequently reducing its heat transfer. The coefficient of overall heat transfer varies with temperature; however, this study shows the average values (Table 4).

Table 4: Coefficient of Overall Heat Transfer of Fresh Water and Saline Water Ice in Table 2 of Paper II

Coefficient of Overall Heat Transfer of Ice (*h*)	**Value (W/(m^2.K))**
Fresh Water Ice	9.2
Saline Water Ice	4.2

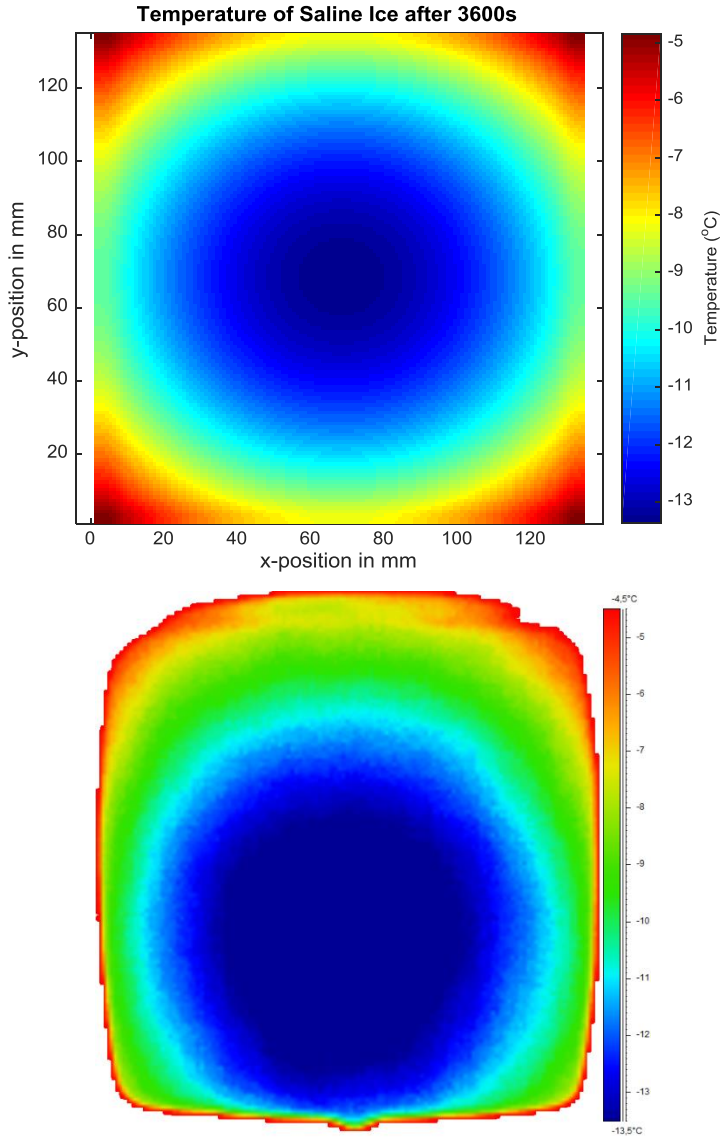

Figure 8: Variation in temperature on the saline water ice cube after 3600s; (a) Finite Difference Method (MATLAB®); (b) False Infrared Image (A310 FLIR®) in Figure 7 of Paper II

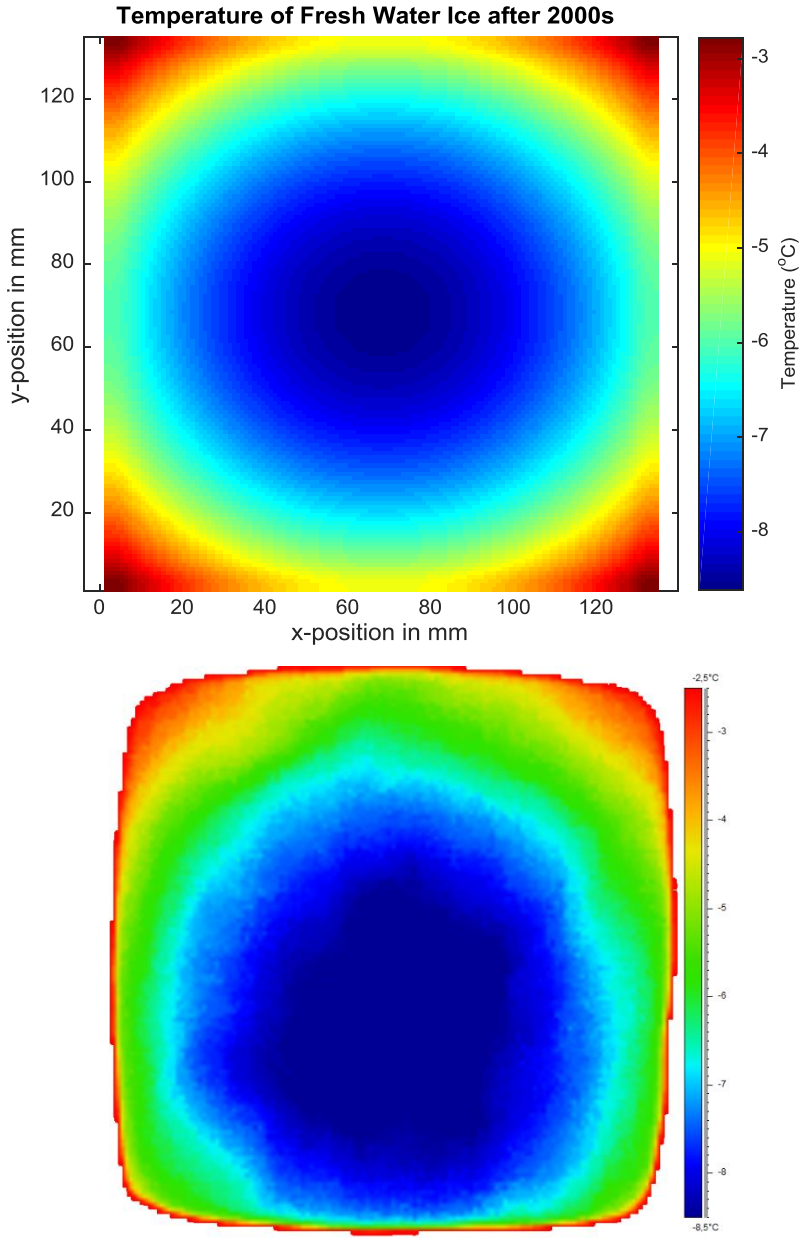

Figure 9: Variation in temperature on the fresh water ice cube after 2000 s;
(a) Finite Difference Method (MATLAB®); (b) False Infrared Image (A310 FLIR®)
in Figure 6 of Paper II

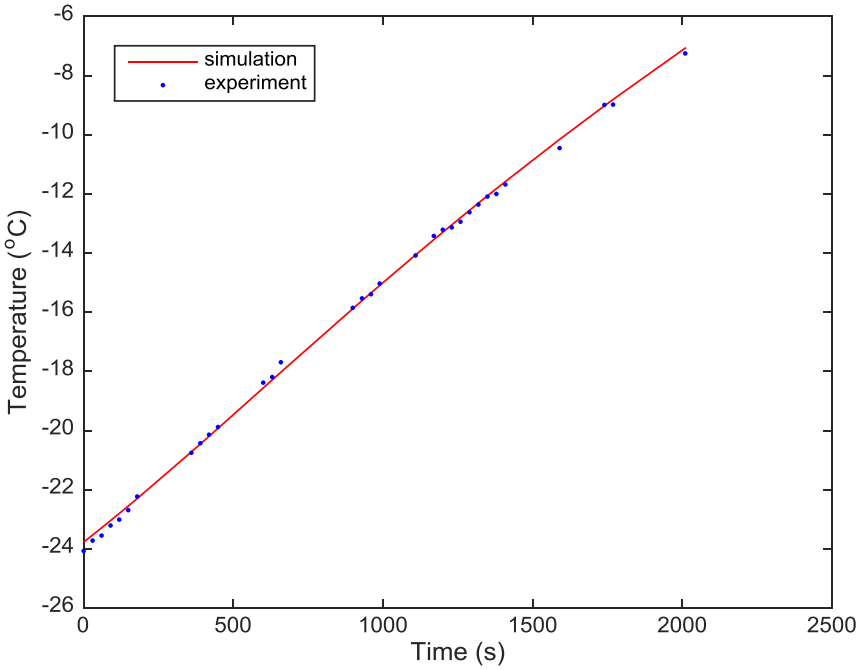

Figure 10: Variation in temperature with time for fresh water ice cube
In Figure 8 of Paper II

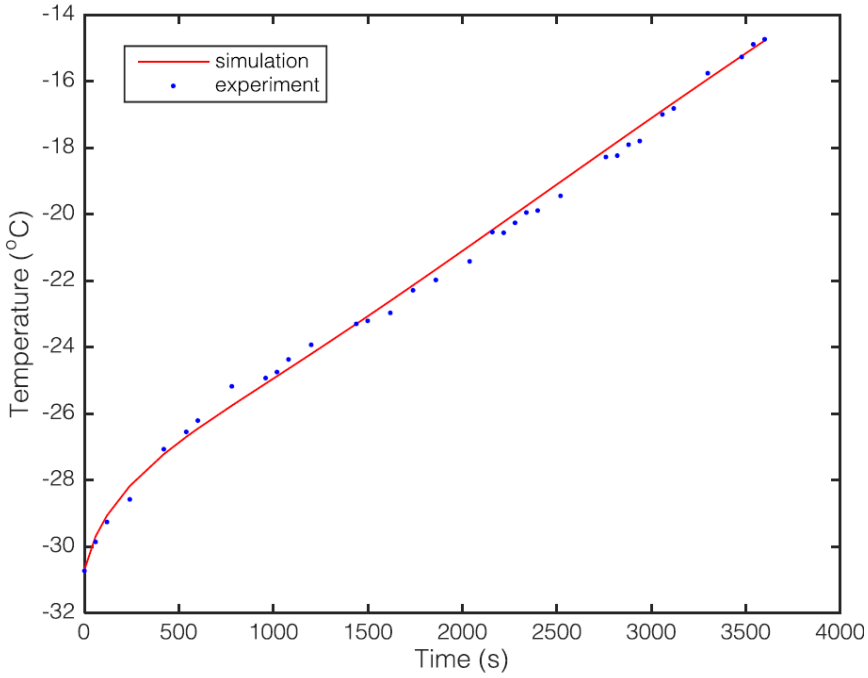

Figure 11: Variation in temperature with time for saline water ice cube
in Figure 9 of Paper II

3.3. Paper III

Marine Thickness of Marine Ice Using IR Thermography
Rashid, T.; Khawaja, H. A.; Edvardsen, K., *Cold Regions Science and Technology 2019*; Vol. 158, pp. 221-229

One of the key research objectives of this study is to measure the marine ice thickness. Real-time information of marine ice thickness on a ship can assist in mitigating the ice accretion. In this study, the marine ice thickness is determined by measuring the surface temperature of the marine icing samples using IRT. This is performed by applying a known external heat source to an icing sample for a certain period of time. The surface temperature of the icing sample is monitored using an IR camera during this period. The heat energy is supplied underneath the icing sample, using a heat source that is in direct contact with an icing sample.

A marine icing sample was prepared on a surface in contact with the heating source. Both are kept at thermal equilibrium state. However, a thermal non-equilibrium state is created as soon as the heat energy is supplied from a heating source. The system tries to attain a thermal equilibrium state and, due to the heat transfer phenomenon, heat energy is transmitted from the heating source to the icing sample. The heat transfer process in a three-dimensional space can be expressed by the heat equation shown in Eq. (9) (Moran, 2003).

$$\frac{\partial T}{\partial t} = \alpha \left(\frac{\partial^2 T}{\partial x^2} + \frac{\partial^2 T}{\partial y^2} + \frac{\partial^2 T}{\partial z^2} \right) \tag{9}$$

where T is the temperature (K), α is the thermal diffusivity term (m^2/s), x, y, z are the spatial dimensions and t is the time (sec).

The heat transfer process causes a temperature distribution within the icing sample. The temperature distribution within the icing sample is $T\ (x, t)$, with x a spatial coordinate (m) and t, time (sec). The marine icing sample under observation is enclosed inside a container with an open top surface, as shown in Figure 12. The heat energy is supplied to the icing sample from beneath. As a result, the surface temperature is changed, due to the heat transfer occurring from the bottom to the top of the icing surface. The change in surface temperature (ΔT) of the icing sample is due to the one-dimensional heat flow. The one-dimensional heat transfer can be expressed by the heat equation shown in Eq. (4):

3.3.1. One-dimensional conductive heat transfer within ice by applying external heat

The mode of heat transfer between the two solid mediums (heating source and marine icing sample) is conduction. This process can be described in terms of an appropriate rate equation, describing the amount of energy being transferred per unit time (heat flux). The rate equation for the conduction is known as Fourier's law, and the heat flux $q_x^{"}$ (W/m^2) in a single dimension with temperature distribution $T(x)$ can be expressed as Eq. (10).

$$q_x^{"} = -k \frac{dT}{dx} \tag{10}$$

The temperature distribution $(\frac{dT}{dx})$ within the icing sample is due to the conditions occurring at the boundaries; i.e., the point of contact of the icing samples with the metallic plate of the heating source, as shown in Figure 12. The conduction process in the icing sample is determined by the temperature distribution within the icing samples. Figure 12 explains the relationship between the heat flux $(q_x^{"})$, temperature distribution $(\frac{dT}{dx})$ and a single-dimensional coordinate system (x-axis) of an icing sample.

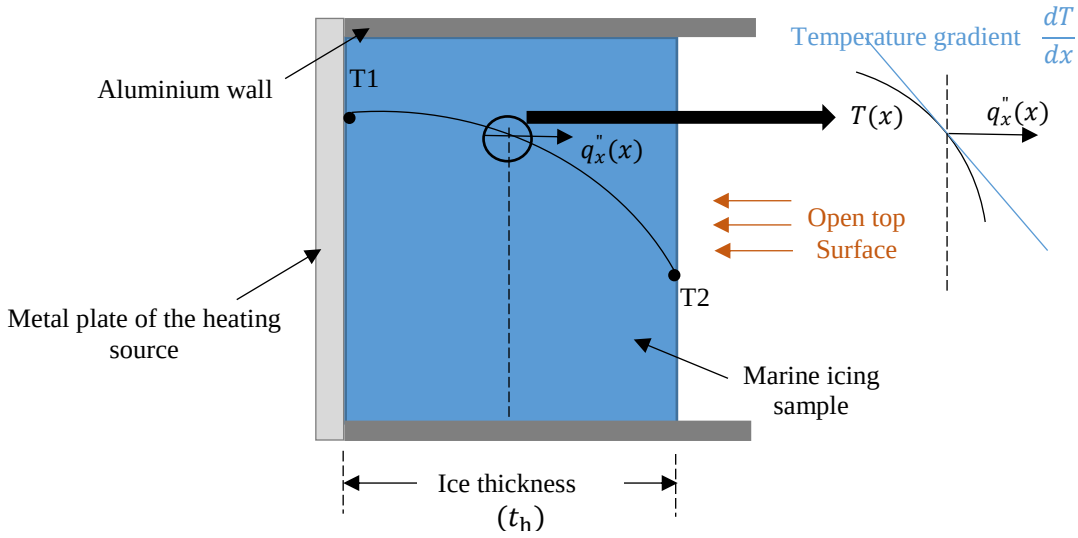

Figure 12: Relationship between heat flux, temperature gradient and coordinate system within an icing sample in Figure 2 of Paper III (adapted from (Moran, 2003))

Provided the boundary conditions are similar, the temperature distribution $(\frac{dT}{dx})$ will change within the icing sample for different thicknesses (t_h). As a result, the temperature (T_2) at the surface of the icing sample will vary. The surface temperatures (T_2) of marine icing samples with different thicknesses $(t_{h1}, t_{h2} \ldots)$ are analysed to address research objective 3. For comparison purposes, similar temperatures (T_1) and environmental conditions are provided for the icing samples.

The thickness (t_h) of the marine icing sample was evaluated in a laboratory-scale experimentation illustrated in Figure 13. The thickness levels of the marine icing samples were analysed as a function of surface temperature gradient ΔT (°C) and time t (sec), as shown in Eq. (11).

$$t_h = f(\Delta T, t) \tag{11}$$

The infrared camera was used to measure the surface temperature gradient (ΔT) of the marine icing samples. The infrared camera measures the changes in surface temperature by capturing its radiation intensity, as described in Eq. (3).

The experimental setup consists of icing containers, a high definition IR camera, cold room, a customized hardware control unit, a software interface and a cold box, as

shown in Figure 13. The sea water was collected from Norskhavet (GPS 69°41'07.2"N 19°00'23.3"E) in order to prepare the marine icing samples. The marine icing samples of different thicknesses, 5mm, 10mm and 15mm, were frozen inside the icing containers in the cold room. The icing samples were taken out of the cold room and put inside the cold box, along with the hardware control unit, as shown in Figure 13. Inside the cold box, the temperature is adjustable down to -55ºC. The experimentation was performed at different temperatures inside the cold box from -15ºC to -30ºC. The infrared camera was mounted on a stand at an angle of 90° to observe the thermal behaviour of the icing samples in the containers when heated from beneath.

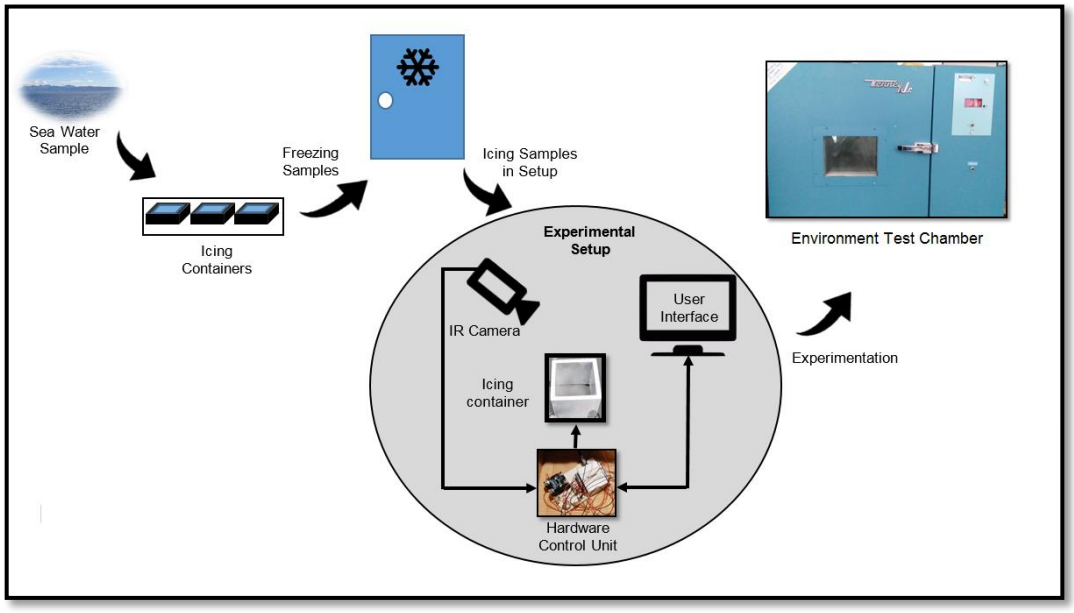

Figure 13: Experimental data collection to measure marine ice thickness in Figure 4 of Paper III

The results presented in Paper III demonstrate the measurement of marine ice thickness using IRT where marine ice is subjected to an externally controlled heating source. The average surface temperature of the marine ice samples shows a particular response when heated inside the cold environment. This particular response (shown in Figure 14) can be acquired by plotting the average surface temperature (T) of the ice against time.

Figure 14 shows three parameters of interest. One is the time (t_0) required for the first significant change in temperature, with respect to the starting temperature (T_o). It is the time calculated immediately after the heating was turned on until the surface temperature of the ice started to rise. The second parameter is the rate of change in the surface temperature $\left(\frac{\partial T}{\partial t}\right)$ of the ice. The third parameter is the time (t_f) taken by the ice sample to reach $\Delta T = 5°C$. It was observed that all these parameters represented a distinct response for different ice thicknesses (t_h).

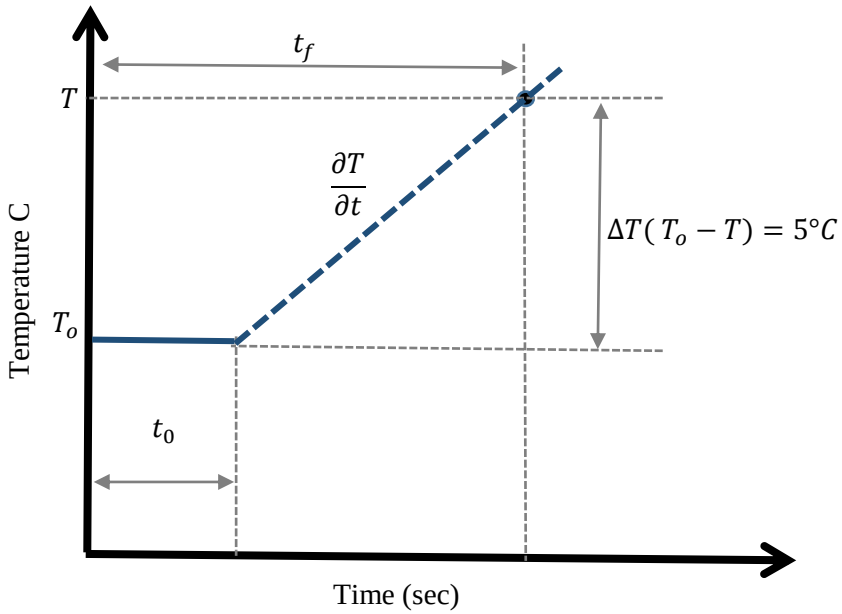

Figure 14: Thermal response of ice surface during heating in Figure 6 of Paper III

The parameters, time to respond (t_0), rate of change of temperature $\left(\frac{\partial T}{\partial t}\right)$, and time to reach ΔT of 5°C (t_f), can be empirically correlated to the initial temperature (T_0) and ice thickness (t_h). It was found that time to respond (t_0) had a strong correlation with ice thickness (t_h).

Three ice samples' thicknesses were selected for comparison (5mm, 10mm and 15mm), as shown in Figure 15. They had a total volume of 2.2cm^3, 4.4 cm^3, and 7.2 cm^3, respectively. These samples were tested for thickness at three different initial temperatures (T_o): -20°C, -25°C and -30°C.

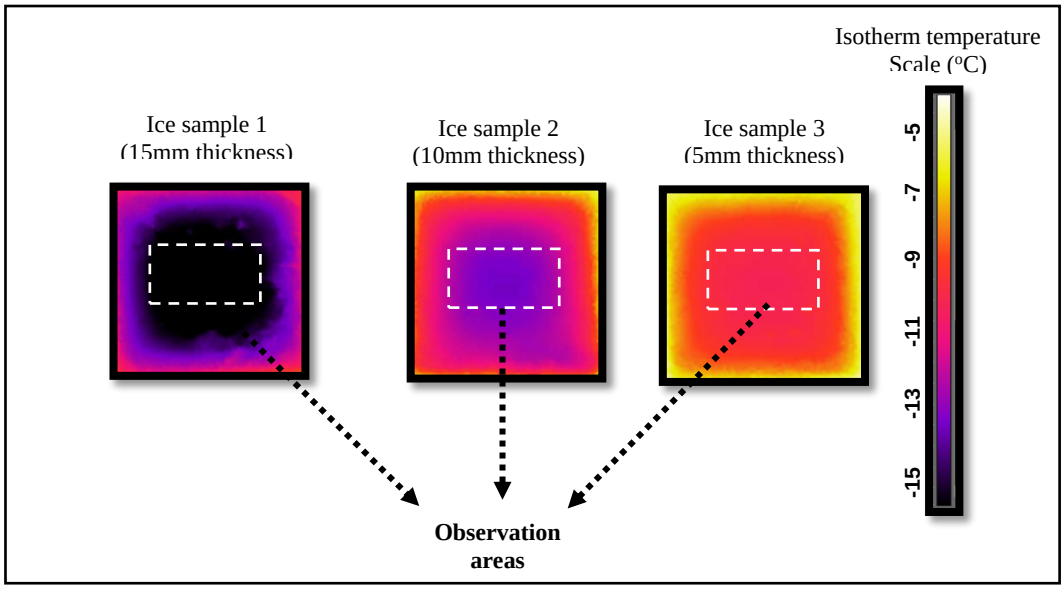

Figure 15: IR images of the surface areas of the ice samples in Figure 7 of Paper III

Table 5 shows a summary of the parameters listed in Figure 14. It presents the numerical values for time to respond (t_0), the rate of change in surface temperature $\left(\frac{\partial T}{\partial t}\right)$ of ice and the time (t_f) taken by the ice to reach $\Delta T = 5°C$. These parameters can be empirically correlated with the ice thickness (t_h). For instance, one of the key results indicates that the time to respond (t_0) for a particular ice thickness has a specific value. This value remains unchanged when the specific ice is heated at different initial temperatures (T_o). The results indicate that the time to respond (t_0) gives a significant indication for measuring the thickness of the ice.

Table 5: The values of $(t_0), (t_f), (\frac{\partial T}{\partial t})$ measured inside a cold environment at different initial temperatures $(T_o = -20°C, -25°C, -30°C)$ in Table 1 of Paper III

Initial Temperature $T_o = -20°C$			
Ice thickness $(t_h)mm$	Rate of change in surface temperature $(\frac{\partial T}{\partial t})\,°C/\text{sec}$	Time to reach $\Delta T = 5°C$ $(t_f)\,sec$	Time to respond $(t_0)\,sec$ $t_o \approx t_f - \frac{5}{(\frac{\partial T}{\partial t})}$
5	0.104	58	9.78 ≈ 10
10	0.068	93	19.82≈ 20
15	0.062	110	29.85≈ 30
Initial Temperature $T_o = -25°C$			
Ice thickness $(t_h)mm$	Rate of change in surface temperature $(\frac{\partial T}{\partial t})\,°C/\text{sec}$	Time to reach $\Delta T = 5°C$ $(t_f)\,sec$	Time to respond $(t_0)\,sec$ $t_o \approx t_f - \frac{5}{(\frac{\partial T}{\partial t})}$
5	0.156	42	9.91≈ 10
10	0.109	66	19.87≈ 20
15	0.1	80	29.78≈ 30
Initial Temperature $T_o = -30°C$			
Ice thickness $(t_h)mm$	Rate of change in surface temperature $(\frac{\partial T}{\partial t})\,°C/\text{sec}$	Time to reach $\Delta T = 5°C$ $(t_f)\,sec$	Time to respond $(t_0)\,sec$ $t_o \approx t_f - \frac{5}{(\frac{\partial T}{\partial t})}$
5	0.185	37	9.95≈ 10
10	0.113	64	19.85≈ 20
15	0.106	77	29.77≈ 30

The time required for the sample to respond (t_0) increases with its thickness (t_h). Table 5 shows that the time (t_0) taken for 15mm is greater (15 seconds), compared to that for 10mm- and 5mm-thick ice (10 seconds and 5 seconds, respectively). It is also observed that t_0 is independent of the starting temperature (T_o).

The rate of change in the surface temperature of ice $\left(\frac{\partial T}{\partial t}\right)$ decreases with its thickness (t_h), as shown in Table 5. For instance, there is a rapid rise in surface temperature of 5mm-thick ice, compared to that of 10mm- and 15mm-thick ice. Considering a specific ice thickness, the rate of change in temperature $\left(\frac{\partial T}{\partial t}\right)$ varies with starting temperature. For instance, $(\frac{\partial T}{\partial t})$ of 10mm ice at (T_o) of $-20°C$ differs from that when (T_o) is $-25°C$ and $-30°C$. Similar behaviour can be observed for the 5mm- and 15mm-thick ice.

Table 5 also shows the values of the time (t_f) taken by the ice to reach a five-degree rise in temperature $(\Delta T = 5°C)$. A direct relationship can be observed between t_f and ice thickness (t_h) at a specific initial temperature (T_o). The time (t_f) increases with increasing ice thickness (t_h). For instance, t_f calculated for a 5mm-thick ice sample is 58 seconds (at $T_o = -20°C$). This value (t_f) is less than that of the 10mm- and 15mm-thick ice ($t_f = 93\ seconds\ and\ t_f = 110\ seconds$), respectively. The rest of the (t_f) values in Table 5 show similar behaviour to that discussed. Considering the variable (T_o), we observe an increase in time (t_f) with a decrease in starting temperature (T_o) for a specific ice thickness (t_h). For instance, the time (t_f) taken by 5mm-thick ice is 37 seconds at $T_o = -20°C$, while, at -25°C and -30°C, t_f is greater, i.e. 42 seconds and 58 seconds, respectively.

Table 6 summarizes the relationship between the correlated parameters. The time (t_0, t_f) and rate of temperature change $\left(\frac{\partial T}{\partial t}\right)$ respond to ice thickness in a specific manner, as described in the discussion above. We observed that (t_0) is the reliable parameter for detecting ice thickness. This is because (t_0) is the time when heat transfer is only happening through the metal surface, adhesive and ice. Essentially, it is due to conduction and is highly predictable, regardless of the environmental conditions. Hence, (t_0) could be a direct means to measure ice thickness. However, (t_0) would be non-linear if ice thickness is considerably large and the initial temperature (T_o) is close to freezing temperatures. The reason for this is the phase change of the ice surface that is in touch with the heating (i.e. ice melts at the heater contact).

The rate of temperature change $(\frac{\partial T}{\partial t})$ is not solely dependent on the conduction phenomenon. It is also dependent on convection on the ice surface. From the heat transfer point of view, $(\frac{\partial T}{\partial t})$ would be non-linear to ice thickness, mainly due to convection. In addition, it will be dependent on the environmental conditions.

The time (t_f) for a five-degree (Celsius) rise $(\Delta T = 5°C)$ is an integral effect of conduction and convection. Similar to $(\frac{\partial T}{\partial t})$, (t_f) would also be non-linear and dependent on the environmental conditions. If (T_o) is not low enough then it would record the effect of phase change (ice melts at the heater contact).

Table 6: Correlation matrix of ice thickness (t_h) with time to respond (t_0), time to reach $\Delta T = 5°C$ (t_f) and rate of change in surface temperature ($\frac{\partial T}{\partial t}$) in Table 2 of Paper III

Variable	**Correlated Parameters**				
	t_0	${t_f}^*$	$\frac{\partial T^*}{\partial t}$		T_0
t_h	**D**	**D**	**I**	**N**	**x**
T_0 (for specific t_h)	**x**	**I**	**I**	**N**	**-**

x = Independent or Weak Relationship D = Direct Relationship
I = Inverse Relationship N= Nonlinear
**subject to environmental conditions*

3.4. Paper IV

Roll to Roll CNT Coating for Electro Thermal Heating
Rashid, T.; Liang, HL.; Chiodarelli, N.; Khawaja, H. A.; Edvardsen, K.; De Volder, M. Manuscript ready.

In this paper, a roll-to-roll (R2R) slot-die coating process for thin film carbon nanotube (CNT) heaters is demonstrated. In this process, a continuous CNT suspension is coated on a PET film substrate, subsequently dried and packaged. This process allows for continuous square-meter-size coating. The electrical resistance and thermal signatures of these samples are measured by high definition infrared (IR) thermography. Anti-/de-icing demonstrations of R2R CNT coated samples are performed inside a cold room and outdoor atmospheric icing conditions.

3.4.1. CNT in thin film preparation

CNT thin films are generally prepared using either solution processing of CNT suspensions or dry spinning methods. Solution-processed CNT films are fabricated by dip coating (Mirri et al., 2012) , spin coating (LeMieux et al., 2008), spray coating (Ramasamy et al., 2008), vacuum filtration (Song et al., 2009), in-jet printing (Kordás et al., 2006) and electrophoretic deposition (Boccaccini et al., 2006). The dry spinning approach relies on the processing of CNT vertically aligned forests (Lepró et al., 2010) and direct spinning methods from a CVD reactor (Li et al., 2004; Sun et al., 2011; Janas and Koziol, 2014). For a more detailed description of these methods, we refer to (Lu et al., 2012). While the dry spinning method has resulted in some of the best film properties and can be implemented in a continuous manufacturing process (Li et al., 2004), it does not profit from the cost benefits of commercial CNTs produced on a large scale. Roll-to-Roll (R2R) coating allows for a cost-effective continuous coating of CNT suspensions. Roll-to-Roll (R2R) coating refers to a family of manufacturing techniques, in which a flexible substrate is coated continuously as it is unwound from a stock roll and transferred to a rewinding roll. This process is particularly suited to large-area coating and has previously been used for coating CNTs in RFID tags (Jung et al., 2010), active matrices for multi-touch sensors (Lee et al., 2015), but, to our knowledge, R2R coating of CNT dispersion has not yet been used for CNT heaters.

Large-area, low-cost heaters are particularly interesting for anti-/de-icing of ships entering the Arctic region. This is due to ship ice accretion caused by sea spray. Icing can affect the ship's operations, risking human and machine safety (Wiersema et al., 2014; Marchenko, 2012). At present, ice on ships is removed manually and/or by applying heat (Samuelsen, 2017), and real-time monitoring of icing parameters (such as ice detection, ice thickness) is being developed (Rashid et al., 2018). This paper shows that continuous CNT films can be coated on PET substrates, using a standard slot-die R2R coating system. These CNTs films have then been used to demonstrate their thermal anti-/de-icing capability.

3.4.2. Methods

A MWCNT ink (Electra Colour™ – CNTBlack) provided by Owen Research was used with varying CNT concentrations. Prior to use, the CNT suspension was sonicated for two hours in a bath sonicator and centrifuged for about 10 min at 8000 rpm. The CNT ink was coated on a PET foil, using slot-die coating on a roll-to-roll coater (Easycoater, Coatema®). The viscosity of the CNT ink was adjusted by varying the surfactant composition, in order to make it suitable for R2R coating. To perform a single coating run on an R2R coater, 250ml of CNT ink was prepared.

The coater was used to coat lengths of to 2 meters at a time, which were then dried at room temperature. A removable protective film was then laminated on the R2R coating for safe handling of the CNT films. For coating, the ink was pumped at a rate of 1.9 ml/min into the slot-die head. The head was fixed at a gap of 1.4 mm from the substrate. The width of the coating was 10 cm. The coating setup is shown in Figure 16a and 16b and a coated sample is shown in Figure 16c. Finally, electrical connections were applied on the CNT films, using RS Pro® silver conductive adhesive paint. Silver tracks were drawn in the CNT coating direction (Figure 16d). Figure 2 shows the complete method of R2R coating and characterization of CNTs on a PET substrate.

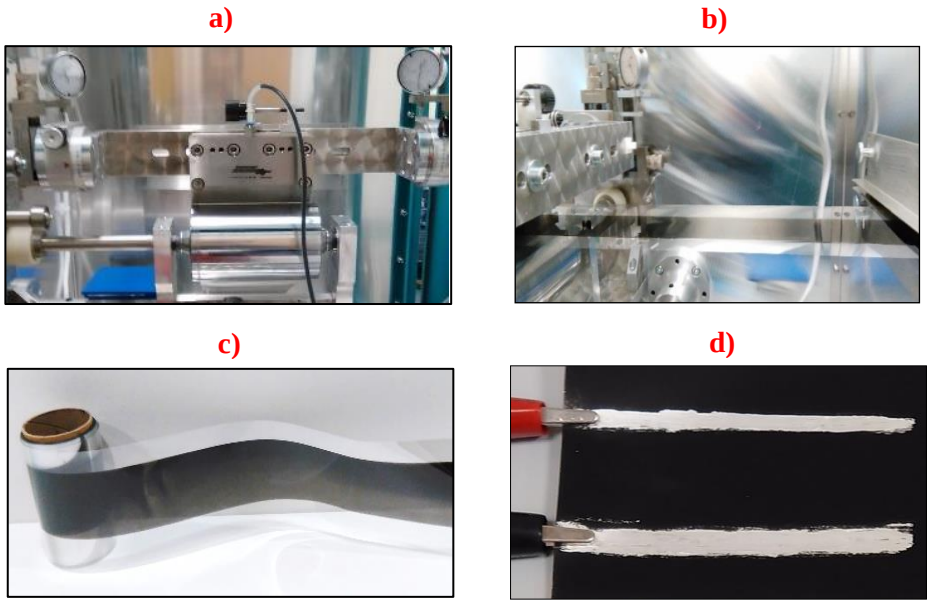

Figure 16: (a) Pumping CNT ink into slot die coating; (b) coating onto PET substrate, (c) CNT coated roll; (d) drawing conductive Ag ink on the CNT coating in in Figure 1 of Paper IV

After coating and connecting the CNT film, a DC electrical power supply (TENMA® 75-8695) was used for joule heating the films. The infrared thermography (IRT) of CNT samples was observed using a high definition infrared camera, FLIR® (T1030Sc). The IR image post processing and analysis was performed using FLIR® ResearchIR software.

Qualitative anti-/de-icing tests were performed on the R2R coated CNT films inside a cold room and outdoors in atmospheric icing conditions. Ice was frozen on the reverse side of the CNT coated film, while the surrounding temperature was -2°C. Similarly, an anti-/de-

icing experiment was performed outdoors. The atmospheric temperature was -1.5ºC with a humidity of 88% (source: www.yr.no).

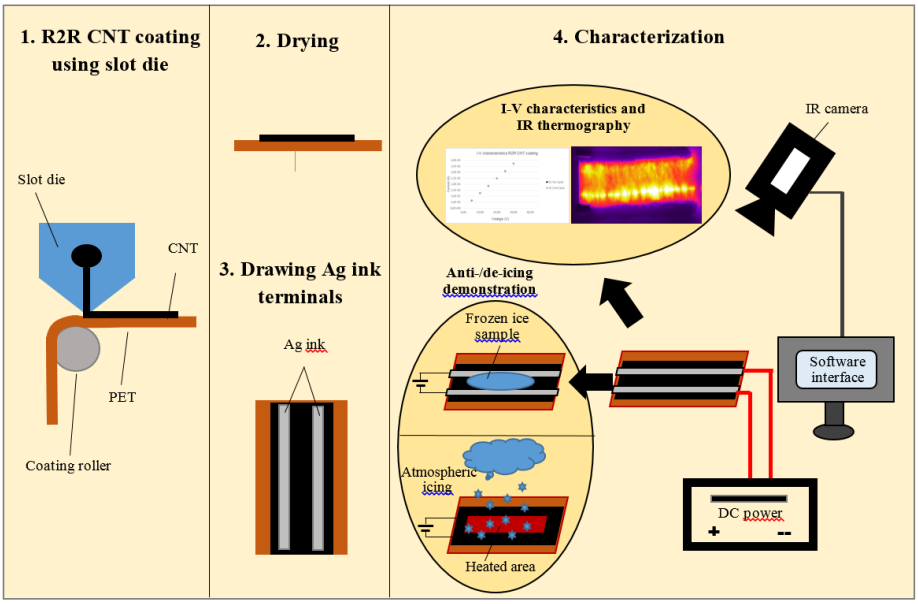

Figure 17: Roll to roll coating and characterization of CNTs on a PET substrate in Figure 2 of Paper IV

3.4.3. Results and Discussion

Four different CNT suspensions (1wt.% to 4wt.%) were processed to obtain coatings, named S1 to S4, respectively. The electrical and thermal response was measured for these samples. Of these samples, only S2 and S3 gave satisfactory results and are presented here. The current and voltage characteristics of samples S2 and S3 are shown in Figure 18. A linear I-V response was obtained for both samples. The electrical resistance values at the terminals of S2 and S3 are found to be 806Ω and 23.2KΩ, respectively.

Figure 19 shows the surface IRT of S2 and S3 at 25V, 30V, and 35V. An average surface temperature of up to 50.3ºC ± 3.8ºC was observed on S2, compared to the 22.8ºC ± 0.7ºC on sample S3 at 35V. A summary of the samples' average surface temperatures, observed at the particular voltages applied, is given in Table 7.

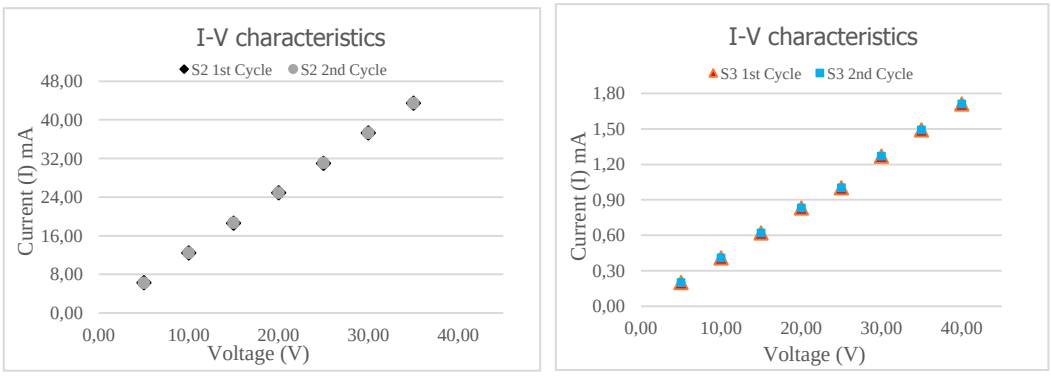

Figure 18: I-V characteristics of R2R CNT coated samples (S2 and S3) in Figure 3 of Paper IV

Table 7: Current and temperature parameters of samples S2 and S3 at different voltages (dc) in Table 1 of Paper IV

Current (I)			Average surface temperature of R2R CNT coated sheet (8.5cm x 3cm)		
Voltage (dc)	**Sample**		**Voltage (dc)**	**Sample**	
	S2	**S3**		**S2**	**S3**
10 V	12.44 mA	0.41 mA	25 V	35.32V±2.7 V	22.10±0.4 V
20 V	24.94 mA	0.83 mA	30 V	42.57±3.6 V	22.72±0.6 V
30 V	37.30 mA	1.27 mA	35 V	50.0±3.8 V	22.84±0.7 V
40 V	-	1.71 mA	40 V	-	23.15±1.0 V

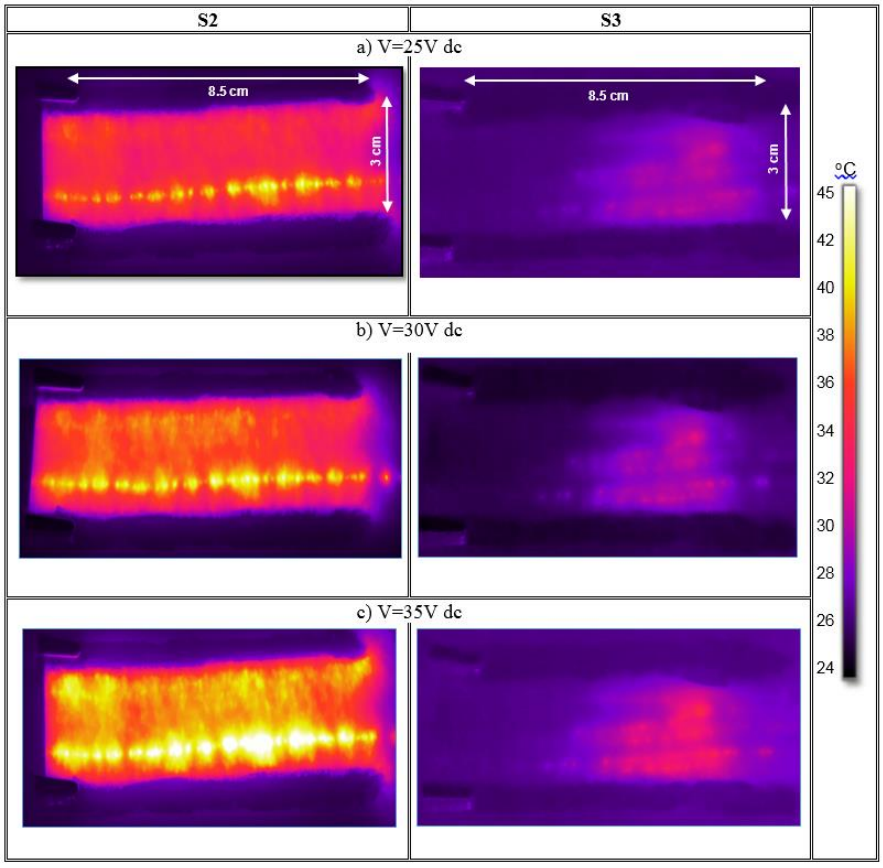

Figure 19: Surface infrared thermography (IRT) of S2 and S3 at a) V=25V dc b) V=30 V dc c) V=35V dc in Figure 4 of Paper IV

A qualitative de-icing demonstration, using the R2R CNT coated sample S2 (area 25.5 cm^2), was performed inside the cold room, as shown in Figure 20. Time-elapsed photos and IR images were taken at 60-second intervals to show the process of de-icing over the

CNT film surface (Figure 20). The IR image of Figure 20a shows the ice and PET sheet at a surrounding temperature of -2°C. Similarly, Figure 21 shows an outdoor de-icing experiment in Tromsø, Norway (25-11-2018, GMT18:20). The coating sample kept the heated area ice-free and prevented further ice accretion (Figure 21 a-c).

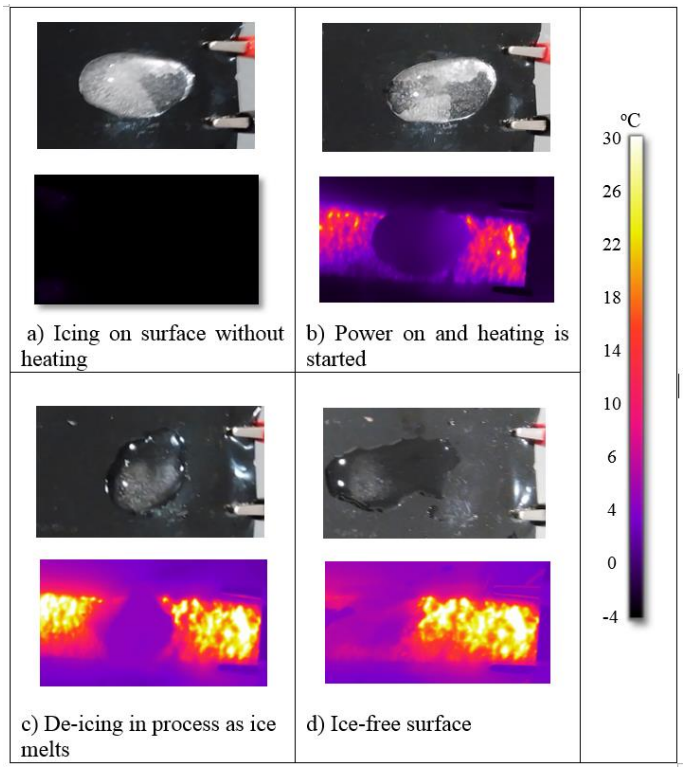

Figure 20: De-icing demonstration of R2R CNT coated sheet (IR and colour images), when ice is frozen inside cold room at steady state temperature of -2°C in Figure 5 of Paper IV

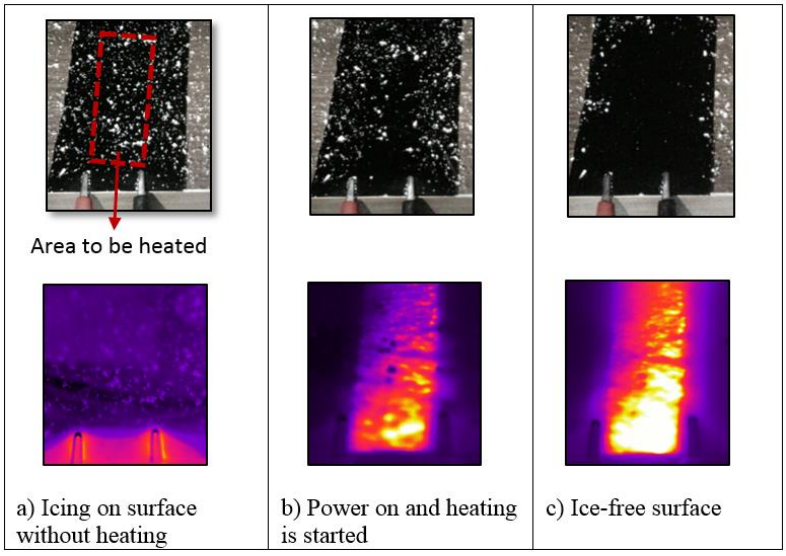

Figure 21: Anti-/de-icing demonstration of R2R CNT coated sheet (IR and colour images) in atmospheric icing conditions (Tromsø, Norway, 25-11-2018, GMT: 18:20) in Figure 6 of Paper IV

3.5. Summary of appended papers

The relationship between the appended papers and the research questions formulated (in this study) can be shown in Table 8, with +++ denoting the strongest and + the weakest relationship. This relationship is also presented in Figure 22.

Table 8. The appended papers addressing the research questions

Paper	Research Question 1	Research Question 2	Research Question 3	Research Question 4
Paper I	+++	+	+	+
Paper II	++	+++	+	-
Paper III	++	++	+++	++
Paper IV	+	++	++	+++

Paper I

This paper mainly contributes to Research Question 1 of this study. The paper's aim is to review the phenomenon of icing in marine operations. In this regard, sea spray icing is discussed, and an overview of the ice accretion prediction models and their fundamental parameters is provided. This paper also reviews the anti-/de-icing technologies that can be implemented in cold climate regions. A brief review of the ice detection technologies is also presented in this paper, in order to understand the various methods to mitigate the icing conditions.

Paper II

Addressing Research Questions 1 and 2 of this study, this paper provides a foundation for adopting infrared thermography (IRT) as a remote monitoring tool to characterize marine ice in comparison with pure ice. The paper has two major parts: experimental results and simulation analysis. The experimental results prove the feasibility of employing IRT to observe marine ice by monitoring thermal gradients on its surface. For comparison purposes, fresh water ice is also observed in similar conditions. The second part of this paper provides the simulation analysis, based on the finite difference method. The simulation analysis validates the experimental results of IRT by confirming the marine and pure ice thermal conductivity and overall heat transfer coefficient.

Paper III

This paper addresses Research Questions 1 to 4 of this study. This paper successfully demonstrates the measurement of marine icing thickness using IRT when icing samples are subjected to control heating from beneath. The marine ice thickness is calculated using laboratory-scale experiment, and the key parameters associated with the marine ice thickness are identified and empirically correlated. The experimentation results show that

time to respond (t_0), rate of change of temperature $\left(\frac{\partial T}{\partial t}\right)$, and time to reach ΔT of 5°C (t_f) can be empirically correlated with initial temperature (T_0) and ice thickness (t_h). It was also demonstrated that time to respond (t_0) had a strong correlation with ice thickness (t_h) and the methodology can be implemented on larger ships that will require setup calibration.

Paper IV

This paper addresses Research Question 1, 2 and 4 of this study. It is demonstrated that the R2R coating of CNT ink on a PET substrate allows for the continuous fabrication of heaters, which show promising properties for this application. CNT suspensions with different viscosities were coated and tested electrically and thermally. In addition, qualitative anti-/de-icing demonstrations are presented, both in a climate chamber and outdoors using natural snow. These heaters, therefore, show promise for the anti-/de-icing of ships in arctic waters.

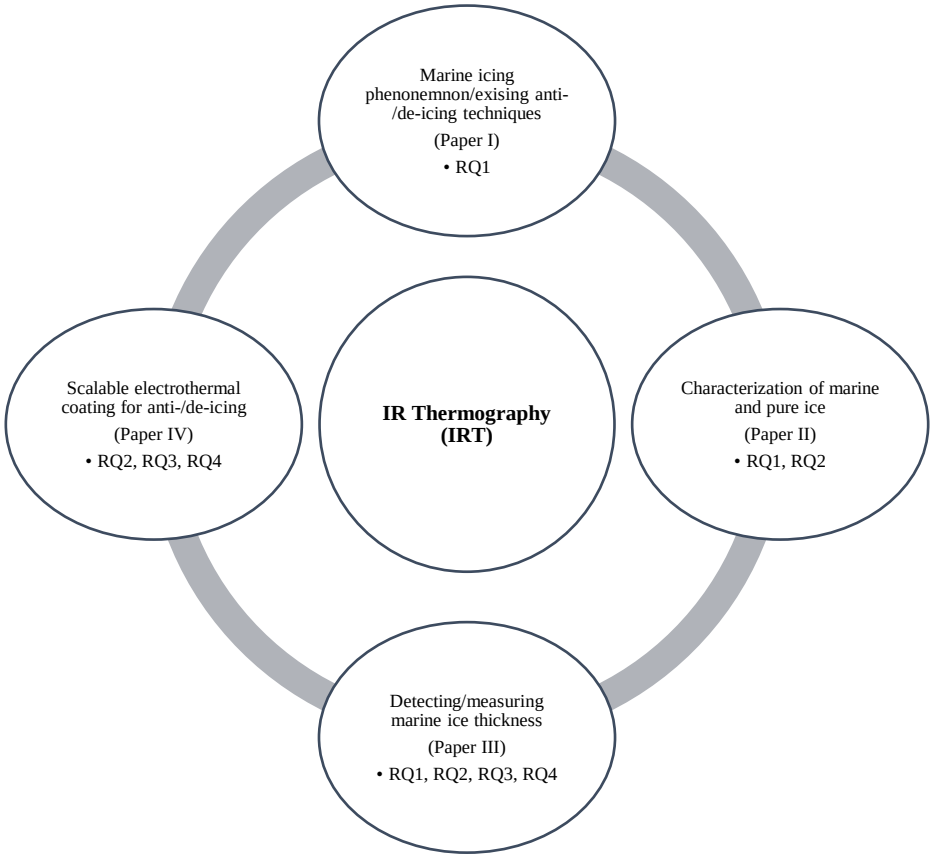

Figure 22: Relationship between the appended papers and research questions

4. Research contributions and suggestions for future work

4.1. Research contribution

This study can be seen as contributing in two major areas: the validation of IRT to remotely monitor marine ice thickness, and the manufacturing of a thermoelectric material that can be used in ships' anti-/de-icing systems. In light of these, the study makes the following scientific contributions:

- The study has demonstrated the potential of infrared thermography (IRT) to observe marine ice in a cold climate environment. The possibility of remotely monitoring marine ice in a controlled environment has been investigated.

- The study has provided a method to measure the thickness of marine icing, using an external heating source. This method can be implemented in any existing and/or modified anti-icing/de-icing system with setup calibration.

- The study has demonstrated the possibility of deploying a customized electrothermal anti-icing/de-icing coating material, manufactured from carbon nanotubes (CNTs). The excellent electrothermal properties of CNT are utilized, and PET sheets are coated with CNTs, using an industrial R2R coater.

4.2. Suggestions for future work

Based on the research presented in this thesis, the following points for future research are suggested:

- The laboratory-scaled prototype to measure marine ice thickness can be scaled up to be tested on a ship. Further work can be done by devising a method to calibrate the setup on a large scale. For instance, the calibration setup will involve further investigation of the thermal distribution of the heating elements used for anti-/de-icing elements, optimal distribution of the target areas, optimal height and distance the infrared camera is placed from the target, and the safety and protection of equipment exposed to the cold climate.

- The electrothermal CNT ink can be further improved to achieve uniform heating over the entire coated area. Thereafter, the coating material can be applied to different areas

of the ship, and real-time marine icing can be observed through IRT combined with active heating.

References

Ayele YZ and Barabadi A. (2016) Risk based inspection of offshore topsides static mechanical equipment in Arctic conditions. *2016 IEEE International Conference on Industrial Engineering and Engineering Management (IEEM).* 501-506.

Barber D, Ehn J, Pućko M, et al. (2014) Frost flowers on young Arctic sea ice: The climatic, chemical, and microbial significance of an emerging ice type. *Journal of Geophysical Research: Atmospheres* 119.

Boccaccini AR, Cho J, Roether JA, et al. (2006) Electrophoretic deposition of carbon nanotubes. *Carbon* 44: 3149-3160.

Comiskey A, Leslie L and Wise J. (1984) Superstructure icing and forecasting in Alaskan waters. *Arctic Environmental information and Data Center. Seattle: University of Alaska*.

Courant R, Friedrichs K and Lewy H. (1928) Über die partiellen Differenzengleichungen der mathematischen Physik. *Mathematische Annalen* 100: 32-74.

Dehghani S, Naterer G and Muzychka Y. (2017) Transient heat conduction through a substrate of brine-spongy ice. *Heat and Mass Transfer* 53: 2719-2729.

Fazelpour A, Dehghani SR, Masek V, et al. (2016) Infrared image analysis for estimation of ice load on structures. *Arctic technology conference*. Offshore Technology Conference.

Fazelpour A, Dehghani SR, Masek V, et al. (2017) Ice load measurements on known Ssructures using image processing methods. *World Academy of Science, Engineering and Technology, International Journal of Electrical, Computer, Energetic, Electronic and Communication Engineering* 11: 907-910.

Fikke S, Ronsten G, Heimo A, et al. (2006) Cost 727: atmospheric icing on structures. *Measurements and Data Collection on Icing: State of the Art, Publication of MeteoSwiss* 75: 1422-1381.

FLIR®. (2016) *Iceberg ahead!* Available at: http://www.flir.eu/marine/display/?id=52805.

Foder MH. (2001) ISO 12494" Atmospheric Icing of Structures" and How to Use It. *Proceedings of the llth International Offshore and Polar Engineering Conference.* Stavanger, Norway, 1-880653.

Gregoris D, Yu S and Teti F. (2004) Multispectral imaging of ice. *Electrical and Computer Engineering, 2004. Canadian Conference on.* IEEE, 2051-2056.

Homola MC, Nicklasson PJ and Sundsbø PA. (2006) Ice sensors for wind turbines. *Cold Regions Science and Technology* 46: 125-131.

Hori M, Aoki T, Tanikawa T, et al. (2013) Modeling angular-dependent spectral emissivity of snow and ice in the thermal infrared atmospheric window. *Applied optics* 52: 7243-7255.

Horjen I. (2013) Numerical modeling of two-dimensional sea spray icing on vessel-mounted cylinders. *Cold Regions Science and Technology* 93: 20-35.

IMO. (2002) Guidelines for ships operating in Arctic ice-covered waters. *IMO Marine Safety Committee Circular 1056 and Marine Environmental Protection Committee Circular 399*. International Maritime Organization.

IMO. (2004) *SOLAS, consolidated edition, 2004: consolidated text of the International Convention for the Safety of Life at Sea, 1974, and its Protocol of 1988 : articles, annexes and certificates*: International Maritime Organization.

IMO. (2015) International Code of Safety for Ships Operating in Polar Waters (Polar Code). International Maritime Organization.

Janas D and Koziol K. (2014) A review of production methods of carbon nanotube and graphene thin films for electrothermal applications. *Nanoscale* 6: 3037-3045.

Jensen Ø. (2008) Arctic shipping guidelines: towards a legal regime for navigation safety and environmental protection? *Polar Record* 44: 107-114.

Jung M, Kim J, Noh J, et al. (2010) All-Printed and Roll-to-Roll-Printable 13.56-MHz-Operated 1-bit RF Tag on Plastic Foils. *IEEE Transactions on Electron Devices* 57: 571-580.

Kachurin L, Gashin L and Smirnov I. (1974) Icing rate of small displacement fishing boats under various hydrometeorological conditions. *Translation into english from Meteorol. Gidrol. (Moscow)*.

Khawaja H, Rashid T, Eiksund O, et al. (2016) Multiphysics simulation of infrared signature of an ice cube. *The International Journal of Multiphysics* 10.

Kordás K, Mustonen T, Tóth G, et al. (2006) Inkjet Printing of Electrically Conductive Patterns of Carbon Nanotubes. *Small* 2: 1021-1025.

Lee W, Koo H, Sun J, et al. (2015) A fully roll-to-roll gravure-printed carbon nanotube-based active matrix for multi-touch sensors. *Scientific Reports* 5: 17707.

LeMieux MC, Roberts M, Barman S, et al. (2008) Self-sorted, aligned nanotube networks for thin-film transistors. *Science* 321: 101-104.

Lepró X, Lima MD and Baughman RH. (2010) Spinnable carbon nanotube forests grown on thin, flexible metallic substrates. *Carbon* 48: 3621-3627.

Li Y-L, Kinloch IA and Windle AH. (2004) Direct spinning of carbon nanotube fibers from chemical vapor deposition synthesis. *Science* 304: 276-278.

Lozowski EP, Szilder K and Makkonen L. (2000) Computer simulation of marine ice accretion. *Philosophical Transactions of the Royal Soc A*: 811–2845.

Lu W, Zu M, Byun J-H, et al. (2012) State of the Art of Carbon Nanotube Fibers: Opportunities and Challenges. *Advanced Materials* 24: 1805-1833.

Makkonen L. (1984) Atmospheric icing on sea structures. Hanover, (NH): US Army Cold Regions Research and Engineering Laboratory, 102.

Makkonen L. (1987) Salinity and growth rate of ice formed by sea spray. *Cold Regions Science and Technology* 14: 163-171.

Marchenko N. (2012) *Russian Arctic Seas: Navigational conditions and accidents*: Springer Berlin Heidelberg.

MAROFF. (2013) Optimization of ship operations in Arctic waters by application of sensor technologies for ice detection, de-icing and weather data. Project description.

MATLAB®. (2015) version 8.5.0.197613. Natick, Massachusetts: The MathWorks Inc.

Mertins HO. (1968) Icing on fishing vessels due to spray. *Marine Observer* 38: 128-130.

Miller AW and Ruiz GM. (2014) Arctic shipping and marine invaders. *Nature Clim. Change* 4: 413-416.

Mirri F, Ma AW, Hsu TT, et al. (2012) High-performance carbon nanotube transparent conductive films by scalable dip coating. *ACS nano* 6: 9737-9744.

Moran MJ. (2003) *Introduction to Thermal Systems Engineering: Thermodynamics, fluid mechanics, and heat transfer*: Wiley.

O'Dowd CD, Varghese S., Scannell C., Ceburnis D., Facchini M.C. (2008) A combined organic-inorganic sea-spray source function. *Geophys Res Lett*. 35. Article Number:L01801

Overland J, Pease C, Preisendorfer R, et al. (1986) Prediction of vessel icing. *Journal of Climate and Applied Meteorology* 25: 1793-1806.

Patankar S. (1980) *Numerical Heat Transfer and Fluid Flow*: Taylor & Francis.

Petrenko V and Whitworth R. (2002) Physics of Ice. Oxford Univ. Press.

Ramasamy E, Lee WJ, Lee DY, et al. (2008) Spray coated multi-wall carbon nanotube counter electrode for tri-iodide (I3-) reduction in dye-sensitized solar cells. *Electrochemistry Communications* 10: 1087-1089.

Ramires ML, Nieto de Castro CA, Nagasaka Y, et al. (1995) Standard reference data for the thermal conductivity of water. *Journal of Physical and Chemical Reference Data* 24: 1377-1381.

Rashid T, Khawaja HA and Edvardsen K. (2016) Ice detection of pure and saline ice using infrared signature. *Sensors & Transducers* 206: 82.

Rashid T, Khawaja HA and Edvardsen K. (2018) Measuring thickness of marine ice using IR thermography. *Cold Regions Science and Technology*.

Rashid T, Khawaja HA, Edvardsen K, et al. (2015) Infrared thermal signature evaluation of a pure and saline ice for marine operations in cold climate. *Sensors & Transducers* 194: 62.

Roebber P and Mitten P. (1987) Modelling and measurement of icing in Canadian waters. Downsview, Ontario: Canadian Climate Centre.

Ryerson CC. (2009) Assessment of superstructure ice protection as applied to offshore oil operations safety. Hanover (NH): US Army Corps of Engineers.

Ryerson CC. (2011) Ice protection of offshore platforms. *Cold Regions Science and Technology* 65: 97-110.

Ryerson CC and Tripp ST. (2014) Managing Offshore Superstructure Icing. *OTC Arctic Technology Conference*. Houston, Texas: Offshore Technology Conference, 16.

Samuelsen EM. (2017) Prediction of ship icing in Arctic waters-Observations and modelling for application in operational weather forecasting. Doctoral Thesis. UiT- The Arctic University of Norway.

Samuelsen EM, Edvardsen K and Graversen RG. (2017) Modelled and observed sea-spray icing in Arctic-Norwegian waters. *Cold Regions Science and Technology* 134: 54-81.

Sawada T. (1962) Icing on ships and its forecasting. *Journal of Japanese Society of Snow and Ice, Tokyo* 24: 12-14.

Sawada T. (1968) Ice accretion on ships in northern seas of Japan. *Journal of the Meteorological Society of Japan. Ser. II* 46: 250-254.

Shea C and Jamieson B. (2011) Some fundamentals of handheld snow surface thermography. *The Cryosphere* 5: 55.

Shellard HC. (1974) The Meteorological Aspects of Ice Accretion on Ships. *Marine Science Affairs* Geneva: World Meteorological Organization, 34.

Song X, Liu S, Gan Z, et al. (2009) Controllable fabrication of carbon nanotube-polymer hybrid thin film for strain sensing. *Microelectronic Engineering* 86: 2330-2333.

Sun D-m, Timmermans MY, Tian Y, et al. (2011) Flexible high-performance carbon nanotube integrated circuits. *Nature Nanotechnology* 6: 156.

Wiersema E, Lange F, Cammaert G, et al. (2014) Arctic Operations Handbook JIP. *OTC Arctic Technology Conference*. Offshore Technology Conference.

Wise JAC, A. L. (1980) Superstructure icing in Alaskan waters. *NOAA Special Report*. Seattle, WA: Pacific Marine Environmental Laboratory.

WMO. (1962) Precipitation Measurements at Sea. Geneva: World Meteorological Organization.

Zakrzewski WP, Lozowski EP and Muggeridge D. (1988) Estimating the extent of the spraying zone on a sea-going ship. *Ocean Engineering* 15: 413-429.

Zhang Y. (1999) *MODIS (Moderate Resolution Imaging Spectrometer), USCB Emissivity Library* Available at: https://icess.eri.ucsb.edu/modis/EMIS/html/em.html.

Part II – Appended Papers

Paper I

Rashid, T.; Khawaja, H. A.; Edvardsen, K. "Review of marine icing and anti-/de-icing systems". *Journal of Marine Engineering and Technology 2016* ;Vol. 15.(2) s. 79-87; DOI: 10.1080/20464177.2016.1216734

Author contributions: The literature review was conducted by Taimur Rashid. Several meetings with Hassan A. Khawaja were carried out in order to establish the focus of the paper, discuss its contents and structure. Thereafter, the first manuscript was prepared by Taimur Rashid, which was improved by Hassan A. Khawaja and Kåre Edvardsen.

Paper II

Rashid, T.; Khawaja, H. A.; Edvardsen, K. "Determination of Thermal Properties of Fresh Water and Sea Water Ice using Multiphysics Analysis". *The International Journal of Multiphysics 2016* ;Vol. 10.(3) s. 277-291; DOI: 10.21152/1750-9548.10.3.277

Author contributions: The experimentations were conducted by Taimur Rashid and improvements were suggested by Hassan A. Khawaja. The numerical simulation model was provided by Hassan Abbas Khawaja and Taimur Rashid performed further experimentations. The manuscript was written by Taimur Rashid and Hassan A. Khawaja. Kåre Edvardsen provided his comments to improve the manuscript.

Paper III

Rashid, T.; Khawaja, H. A.; Edvardsen, K. "Marine thickness of marine ice using IR thermography". *Cold Regions Science and Technology 2019*; Vol. 158, pp. 221-229; DOI: 10.1016/j.coldregions. 2018.08.025.

Author contributions: Taimur Rashid initiated the main idea and performed initial experiments. The idea was further discussed with Hassan A. Khawaja. The detailed experimentation, data collection and analysis were conducted by Taimur Rashid. The results of this study were discussed with Hassan A. Khawaja and Kåre Edvardsen who contributed by suggesting some improvements. The initial manuscript was written by Taimur Rashid. Hassan A. Khawaja and Kåre Edvardsen provided feedback regarding further improvements in the manuscript.

Errata: Correct figure numbers referred in the text are given below Journal CRST, Vol. 158 (2019), pp. 221-229.

Incorrect figure no. referred in the text	**Journal Page no.**	**Section**	**Correct figure no.**
Fig. 5	222	2. Methodology	Fig. 3
Fig. 2	223	2.1.1. LWIR camera	Fig. 3
Fig. 5	223	2.1.3. Environmental test chamber	Fig. 3
Fig. 2	223	2.1.4. Ice containers	Fig. 3
Fig. 4	226	2.2. Operating cycle	Fig. 5
Fig. 8, Figure and Fig. 10	227	3. Results and Discussion	Figs. 8, 9, and 10
Fig. 1	228	3. Results and Discussion	Fig. 5

Paper IV

Rashid, T.; Liang, HL.; Chiodarelli, N.; Khawaja, H. A.; Edvardsen, K.; De Volder, M. " Roll to Roll coating of carbon nanotube films for electro thermal heating".; Manuscript ready

Author contributions: The main idea of this paper is developed is close cooperation with Michael De Volder (IFM, University of Cambridge, UK). Taimur Rashid performed initial experimentation to validate the idea. The initial results were discussed with Michael De Volder and Hassan A. Khawaja. The material preparation and characterization was done by Taimur Rashid. Dr. Hsin-ling Liang and Dr. Nicolò Chiodarelli provided feedback on the characterization results. Michael De Volder suggested improvements in the characterization. Improvements were performed by Taimur Rashid. The initial manuscript was written by Taimur Rashid which was later modified by Michael De Volder. Improvements in the manuscript were suggested by Hassan A. Khawaja, Kåre Edvardsen and Dr. Nicolò Chiodarelli. The manuscript was finalised by Taimur Rashid and proof read by Michael De Volder.